North Atlantic Rossby Wave Breaking during the Hurricane Season: Association with Tropical and Extratropical Variability

GAN ZHANG[a] AND ZHUO WANG

Department of Atmospheric Sciences, University of Illinois at Urbana–Champaign, Urbana, Illinois

(Manuscript received 14 May 2018, in final form 17 March 2019)

ABSTRACT

This study explores the connection of Rossby wave breaking (RWB) with tropical and extratropical variability during the Atlantic hurricane season. The exploration emphasizes subtropical anticyclonic RWB events over the western North Atlantic, which strongly affect tropical cyclone (TC) activity. The first part of the study investigates the link between RWB and tropical sea surface temperature (SST) variability. Tropical SST variability affects tropical precipitation and modulates the large-scale atmospheric circulation over the subtropical Atlantic, which influences the behaviors of Rossby waves and the frequency of RWB occurrence. Meanwhile, RWB regulates surface heat fluxes and helps to sustain SST anomalies in the western North Atlantic. The second part of the study explores the connections between RWB and extratropical atmosphere variability by leveraging weather regime analysis. The weather regimes over the North Atlantic are closely associated with RWB over the eastern North Atlantic and western Europe, but show weak associations with RWB over the western North Atlantic. Instead, RWB over the western basin is closely related to the weather regimes in the North Pacific–North America sector. The finding helps clarify why the correlation between the Atlantic TC activity and the summertime North Atlantic Oscillation is tenuous. The relations between the extratropical weather regimes and tropical climate modes are also discussed. The findings suggest that both tropical and extratropical variability are important for understanding variations of RWB events and their impacts on Atlantic TC activity.

1. Introduction

Atlantic tropical cyclone (TC) activity is subject to the impact of various weather and climate processes. Prominent climate modes in the tropics, such as El Niño–Southern Oscillation (ENSO) (Bjerknes 1969) and the Atlantic meridional mode (AMM) (Chiang and Vimont 2004), exert strong influences on the seasonal activity of Atlantic TCs (e.g., Gray 1984a; Vimont and Kossin 2007). The relation inspired extensive investigations of the tropical controls of Atlantic TC activity (e.g., Goldenberg and Shapiro 1996; Zhang and Wang 2013; Patricola et al. 2014) and laid the foundation for the seasonal prediction practice (e.g., Gray 1984b; Vitart et al. 2007; Vecchi et al. 2014). Besides the tropical controls, there has been long-held interest in how extratropical circulation anomalies may affect Atlantic TC activity (Ballenzweig 1959). For example, equatorward-intruding upper-level troughs can affect TC intensification (e.g., Molinari and Vollaro 1989; Hanley et al. 2001; Leroux et al. 2016; Peirano et al. 2016; Fischer et al. 2017) or promote TC genesis (e.g., Davis and Bosart 2004; Galarneau et al. 2015; Bentley et al. 2017). However, studies of the leading mode of extratropical circulation, the North Atlantic Oscillation (NAO), led to inconsistent conclusions about whether and how the NAO affects Atlantic TC activity (Elsner 2003; Sabbatelli and Mann 2007; Kossin et al. 2010; Colbert and Soden 2012; Murakami et al. 2016). Despite the evident challenge, reconciling the tropical and extratropical controls is important for understanding Atlantic TC activity.

Recent studies (Zhang et al. 2016, 2017; Bentley et al. 2017; Papin 2017; Li et al. 2018) have highlighted that Atlantic TC activity is closely associated with Rossby wave breaking (RWB; McIntyre and Palmer 1983; Appenzeller and Davies 1992; Thorncroft et al. 1993). During the hurricane season, *anticyclonic* RWB events occur often in the subtropics and over the TC-prone

[a] Current affiliation: Atmospheric and Oceanic Sciences Program, Princeton University, and NOAA/Geophysical Fluid Dynamics Laboratory, Princeton, New Jersey.

Corresponding author: Gan Zhang, ganzhang@princeton.edu

DOI: 10.1175/JCLI-D-18-0299.1

TABLE 1. Correlation between an RWB index and climate indices (Jul–Oct of 1979–2013). The RWBw index is defined as the seasonal frequency of RWB occurrence over the northwestern subtropical Atlantic [the Dw domain in Zhang et al. (2017)]. MDR denotes SST in the main development region of Atlantic TCs (10°–20°N, 20°–90°W; Goldenberg et al. 2001); AMM and PMM denote the indices of Atlantic meridional mode and Pacific meridional mode, respectively (Chiang and Vimont 2004). The Niño-3.4 and Niño-4 indices are the SST average over 5°N–5°S, 120°–170°W and 5°S–5°N, 160°E–150°W, respectively. NAO/CPC and NAO/Jones follow the definitions by Barnston and Livezey (1987) and Jones et al. (1997), respectively. The east Atlantic (EA) pattern is defined by Barnston and Livezey (1987). The correlation coefficients exceeding the 95% confidence level are in bold.

	MDR	AMM	PMM	Niño-3.4	Niño-4	NAO/CPC	NAO/Jones	EA
RWBw	**−0.67**	**−0.65**	0.25	0.29	**0.33**	0.32	**0.38**	**−0.41**

western basin (Zhang et al. 2017). Those events are associated with extratropical Rossby wave trains and the amplification of an upper-level ridge near the east coast of North America (Zhang and Wang 2018). In the upper troposphere and lower stratosphere, the anticyclonic RWB events show that an air mass of low potential vorticity (PV) and an air mass of high PV rotate around each other anticyclonically (e.g., Thorncroft et al. 1993). In particular, the anticyclonic RWB events are associated with the equatorward intrusions of upper-level troughs and extratropical dry air. The environmental anomalies associated with the extratropical intrusions tend to suppress the tropical convection, with an exception along the leading edge of the trough (Zhang et al. 2017; Bentley et al. 2017). The impact manifests on the seasonal time scale, and the interannual correlation between the indices of RWB occurrence and Atlantic TC activity is significant and negative (Zhang et al. 2017; Papin 2017). Notably, the strong correlation is comparable to those between Atlantic TC activity and the tropical SST (Zhang et al. 2017). While tropical SST was generally considered as the leading control of Atlantic TC activity (e.g., Patricola et al. 2014; Vecchi et al. 2014), regional model experiments suggested that extratropical processes play an important role in modulating Atlantic TC activity and that their impacts may exceed the direct impacts of local tropical SST in some years (Chang and Wang 2018).

The recent findings of the RWB–TC relation raise new questions on the physical controls of Atlantic TC activity. On the one hand, the frequency of *anticyclonic* RWB occurrence shows significant correlations with the tropical Atlantic SST and the tropical Pacific SST on the interannual scale (Zhang et al. 2017; Table 1). The correlations invite investigations of possible *extratropical–tropical interactions*. For example, do these correlations arise because the tropical SSTs dictate the atmosphere circulation and thus the frequency of RWB occurrence? Or could RWB events actively affect the tropical SST via interactions at the air–sea interface? On the other hand, Zhang et al. (2016, 2017) suggest that the variations of RWB events are related to *extratropical atmospheric variability* during the hurricane season, but the frequency of RWB occurrence only shows weak correlations with the NAO and the east Atlantic mode (Table 1). The weak correlations, as well as the obscure NAO–TC relation (Elsner 2003; Kossin et al. 2010; Colbert and Soden 2012; Murakami et al. 2016), highlight the need to clarify the physical relation between RWB events and extratropical atmosphere variability. Accordingly, the rest of the introduction will be organized under the themes of extratropical–tropical interactions and extratropical atmosphere variability.

Tropical climate modes, such as ENSO and the AMM, modulate tropical precipitation and atmospheric circulation. The atmospheric responses can span over both the tropics (e.g., Gill 1980) and the extratropics (e.g., Sardeshmukh and Hoskins 1988; Trenberth et al. 1998; Rodwell and Hoskins 2001; Held et al. 2002). Variations of the basic state of the atmospheric flow, such as the barotropic wind shear, regulate behaviors of Rossby waves and RWB (e.g., Thorncroft et al. 1993; Peters and Waugh 1996; Hartmann and Zuercher 1998; Orlanski 2003). Earlier studies also suggest that the ENSO affects the large-scale environment and contributes to variations of RWB events that influence the west coast of North America (e.g., Orlanski 2005; Ryoo et al. 2013) and the North Atlantic (e.g., Drouard et al. 2015). Although most of those studies focus on the cold season, responses of the atmospheric flow to tropical precipitation variations are also present during the warm season. Cassou et al. (2005) showed that the diabatic heating associated with the Caribbean and Sahelian precipitation can change the statistics of the weather regimes over the extratropical North Atlantic. Sutton and Hodson (2005, 2007) showed that the SST of the tropical North Atlantic modulates the Caribbean precipitation and affects the seasonal climate of western Europe. Notably, those studies leveraged ensemble simulations to study extratropical responses, as the tropics-forced responses in the extratropics are relatively small in comparison with the unforced variability of the extratropical atmosphere (Sutton and Hodson 2007).

Meanwhile, mounting evidence also suggests that variations of extratropical atmosphere can contribute to

the variability of tropical ocean and precipitation. On the synoptic to intraseasonal time scales, equatorward-propagating atmospheric perturbations, such as breaking Rossby waves, can modulate tropical precipitation and tropical atmosphere variability (Ferranti et al. 1990; Kiladis 1998; Funatsu and Waugh 2008; Ray and Zhang 2010), including the warm-season precipitation in the Atlantic basin (Tomaziello et al. 2016; Vigaud and Robertson 2017; Zhang et al. 2017; Li et al. 2018). In addition, the near-surface perturbations associated with extratropical weather systems regulate heat and momentum fluxes at the air–sea interface, which can affect the underlying ocean and contribute to the SST variability (e.g., Strong and Magnusdottir 2009; Häkkinen et al. 2011). The variations of air–sea fluxes tend to be stronger during the cold season but are also evident during the warm season (e.g., Strong and Magnusdottir 2009; Dong et al. 2013). On the monthly to interannual time scales, the oceanic responses in the extratropics can extend to the low latitudes via the interaction between low-level wind and surface heat fluxes (Chiang and Bitz 2005; Alexander et al. 2010; Smirnov and Vimont 2012), as well as adjustments of the gyre circulation and the meridional overturning circulation of the ocean (Barrier et al. 2014). The oceanic anomalies that slowly extend from the extratropical North Atlantic to the low latitudes are important for skillful multiyear predictions of the tropical Atlantic atmosphere (Dunstone et al. 2011) and TC activity (Smith et al. 2010). Nonetheless, it is unclear how the tropical Atlantic Ocean might respond to extratropical weather anomalies on the synoptic time scale during the hurricane season.

Many aspects of extratropical atmosphere variability have been connected to variations of RWB events. Past studies on wintertime RWB have emphasized the role of RWB events in the phase transition and maintenance of the NAO (e.g., Benedict et al. 2004; Franzke et al. 2004; Rivière and Orlanski 2007; Woollings et al. 2008; Strong and Magnusdottir 2008; Drouard et al. 2015). RWB has also been linked to atmospheric blocking events (e.g., Tyrlis and Hoskins 2008) and wintertime weather regimes, such as the Atlantic ridge and the Scandinavian blocking (Michel and Rivière 2011; Swenson and Straus 2017). The relation between RWB and the extratropical atmosphere variability (e.g., the NAO) depends on whether RWB-associated anomalies and atmospheric modes are spatially aligned (Strong and Magnusdottir 2008). Furthermore, the midlatitude atmospheric circulation anomalies over the North Pacific can affect the propagation of Rossby waves and their breaking over the North Atlantic in winter (e.g., Franzke et al. 2004; Drouard et al. 2013, 2015). Those physical mechanisms may also operate during the Atlantic hurricane season, even though their manifestation could differ due to seasonal changes of the atmospheric circulation. A careful investigation of the relation between RWB events and the NAO, as well as other circulation patterns revealed by weather regimes analysis, will likely be enlightening.

By leveraging the fundamental understanding of those weather–climate processes, this exploratory study seeks to answer the following questions: 1) *What are the physical connections between anticyclonic RWB and the tropical climate modes, such as the AMM and ENSO?* 2) *What extratropical processes may affect variations of anticyclonic RWB events, especially the events over the western Atlantic?* The rest of this study is organized as follows. Section 2 introduces the data and tools used for analyses. Section 3 explores the physical connections involving variations of RWB and tropical climate modes. Section 4 investigates the relation between variations of the RWB events and extratropical atmosphere variability. Section 5 provides a summary and discussion of the results.

2. Data and methodology

a. Reanalysis and observational data

The study uses both the monthly and the 6-hourly data from the ERA-Interim dataset (Dee et al. 2011). The ERA-Interim monthly data, together with the Hadley Centre Sea Ice and Sea Surface Temperature (HadISST) dataset (Rayner et al. 2003), Global Precipitation Climatology Project (GPCP) dataset (Adler et al. 2003), and the Atlantic hurricane database (Landsea and Franklin 2013), is used to examine seasonal variations of the large-scale environment. The ERA-Interim 6-hourly data are regridded to a 2.5° grid and used to identify RWB and examine the associated synoptic variations. The identification of RWB is conducted on the 350-K isentropic surface, which is near the 200-hPa level and the tropopause. We search for the meridional reversal of circumglobal PV contours and categorize the features as cyclonic and anticyclonic RWB based on the rotation direction of air masses (e.g., Thorncroft et al. 1993). More details of the reanalysis data, as well as the RWB identification algorithm (Strong and Magnusdottir 2008), have been described in companion studies (Zhang et al. 2016, 2017; Zhang and Wang 2018). An addition in this study is the 6-hourly data involving the air–sea interaction, including surface temperature, heat fluxes, and wind from the ERA-Interim reanalysis. Although the heat flux data are subject to uncertainties, their quality is among the best of the current-generation surface flux products (Brunke et al. 2011).

For consistency with the companion studies (Zhang et al. 2016, 2017), this study examines the peak of Atlantic hurricane season (July–October) during 1979–2013. From this point, we focus on the *anticyclonic* RWB events. We are particularly interested in the anticyclonic events with high-PV tongues over the western subtropical Atlantic [approximately 20°–35°N, 45°–85°W; see Fig. 1 in Zhang and Wang (2018)]. These events have relatively strong impacts on Atlantic TC activity (Zhang et al. 2017) and will be denoted as RWBw events. We will use composite analysis to study seasonal-mean environmental variations and synoptic-scale variations that are associated with the RWBw events. From the perspective of wave–mean flow interactions, the seasonal mean and synoptic variations can be approximately considered as variations of the basic-state flow and different types of wave perturbations, respectively. We study the variations by examining the differences between sample groups or the anomalies from the climatology. The statistical significance of the differences and anomalies is tested using the Student's *t* test. Unless otherwise specified, we present the statistical significance with the 95% confidence level highlighted for the seasonal-mean variations and the 90% confidence level highlighted for the high-frequency variations, respectively. The choice helps to reveal spatially coherent patterns that are sometimes contaminated by the noise in the unfiltered 6-hourly data.

b. Weather regime analysis

To characterize extratropical atmosphere variability, we follow earlier studies of weather regimes (e.g., Cassou et al. 2005; Swenson and Straus 2017) and apply *K*-means clustering to the 500-hPa geopotential height anomalies. The 200-hPa geopotential height anomalies are also analyzed, but we will mainly discuss the 500-hPa anomalies to be consistent with previous studies on weather regime analysis. We define the anomalies using 6-hourly data by removing the climatological seasonal cycle and the seasonal means in individual years. The definition helps separate seasonal-scale variations—which are related to the basic state of atmospheric flow—from intraseasonal and synoptic perturbations that show stronger variance (Schubert et al. 2011). The high-frequency perturbations are the focus of the clustering analysis. Compared to the empirical orthogonal function analysis, the clustering analysis does not require the orthogonality of modes, which may introduce artifacts into nondominant modes (e.g., Lian and Chen 2012). Avoiding this orthogonality constraint is useful for investigating the RWBw events, since those events are not necessarily associated with the dominant modes of the extratropical atmosphere.

The clustering analysis is applied to the North Atlantic (20°–80°N, 90°W–30°E) and the North Pacific–North America domains (20°–80°N, 150°E–60°W), respectively. The former domain follows the definition by Cassou et al. (2005), and the latter domain aims to cover the upstream precursors associated with the RWBw events (Zhang and Wang 2018). The domains aim to capture the variations of large-scale circulation, and changing the boundaries by 10° does not change the results qualitatively. We initialize the *K*-means clustering using specified clustering centers and iterate 25 times. Random initializations and additional iterations do not change the patterns of weather regimes qualitatively. Common to many clustering methods, the selection of the cluster numbers (K) involves some subjectivity. For the North Atlantic domain, we set the K value to 4 based on our own experiments and the early studies (e.g., Cassou et al. 2005). For the North Pacific/North America domain, we did not find any preceding studies on summertime weather regime. We tested K values ranging from 2 to 8 and set the K value to 6 to derive clusters because the resultant clusters have relatively small total within-cluster variance and show physically interpretable spatial patterns (section 4).

After identifying the weather regimes, we use the composite analysis to characterize their associations with RWB events. For the weather regimes in the North Atlantic domain, we show distributions of RWB events in the same domain with no time lag. For the weather regimes in the North Pacific–North America domain, we examine the Atlantic wave breaking events that lag the weather regimes by 5 days. The 5-day lag is applied because the midlatitude wave perturbations take about 5 days to propagate from the North Pacific to the North Atlantic (Zhang and Wang 2018). Varying the lag value between 3 and 7 days does not qualitatively affect the results, and signatures gradually attenuate when the lag value is increased beyond 7 days.

c. Idealized model simulations

The observational analysis helps reveal connections between the anticyclonic RWB events and environmental variations, but the causality can be obscure. To deal with the limitation while constraining the complexity related to parameterized model physics, we carry out idealized model experiments using the GFDL dry spectral model (Gordon and Stern 1982), which solves the primitive equations. For the simplicity of model simulations, the topography, moist processes, and radiative processes are not included. We run the model at the T42 resolution (64×128 grid) with 20 evenly spaced sigma levels. The output is interpolated to isobaric levels for analysis. The simple model may not reproduce every aspect of observations with great fidelity, such as the potentially important impact of moist diabatic processes on RWB (Zhang and Wang 2018). However, simple models have proven

useful to understand basic behaviors of RWB (e.g., Thorncroft et al. 1993; Peters and Waugh 1996; Hartmann and Zuercher 1998) and upstream precursors of RWB (e.g., Franzke et al. 2004; Drouard et al. 2013).

We note that the physical processes excluded from the idealized model are necessary to maintain the three-dimensional climatological flow, and a realistic basic-state flow is essential for studying wave–flow interactions. To acquire such a basic flow, we estimate the forcing from the excluded model physics by initializing the model with the observed atmospheric state (July–October) and integrating the model for one time step. The differences between the initial state and the ensuing time step are considered as the forcing related to the excluded physical processes. The forcing is then included as a constant term in our experiments and used to maintain a steady basic-state flow. The technique was discussed in Hall (2000) and Franzke et al. (2004) and has proved useful in studying atmospheric responses to tropical forcing (Rodwell and Hoskins 2001; Yoo et al. 2012) and upstream impacts on extratropical RWB (Franzke et al. 2004). Besides maintaining a steady basic-state flow, the technique also introduces an artificial nonlinear term related to transient eddies [section 2c in Franzke et al. (2004)] and is thus unfit for studying climate equilibria. We focus on short simulations (<20 days), during which the technique could represent the evolution of the upper-level flow and RWB in a relatively realistic way (Franzke et al. 2004).

Our tropical forcing experiment, which is similar to that in Yoo et al. (2012), investigates circulation responses to idealized tropical heating at various locations. We define an idealized heating function as

$$H = AC_{\varphi,\theta}C_p, \tag{1}$$

where A represents the maximum heating and is set to $\pm 1.0\,\mathrm{K\,day^{-1}}$. In the tropics, the value corresponds to precipitation variations of $2\,\mathrm{mm\,day^{-1}}$ (Ling and Zhang 2013) and is comparable to observed interannual (section 3a) and intraseasonal (section 5) variations of precipitation. The heating structure is specified with the following function:

$$C_{\varphi,\theta} = \exp\left[\frac{-0.2\times(\varphi-\varphi_0)^2}{D^2}\right]\exp\left[\frac{-0.2\times(\theta-\theta_0)^2}{D^2}\right], \quad \text{if} \quad \frac{(\varphi-\varphi_0)^2+(\theta-\theta_0)^2}{D^2}<4, \tag{2}$$

$$C_p = \sqrt[2]{\cos\left(\frac{p-p_0}{p_1}\pi\right)}, \quad \text{if} \quad 200 \le p \le 900\,\mathrm{hPa}, \tag{3}$$

where φ, θ, and p stand for longitude, latitude, and pressure, respectively. Beyond the specified ranges, the coefficients $C_{\varphi,\theta}$ and C_p are set to zero. The subscript 0 denotes the reference variables. The reference variables determine the center of heating, and the horizontal range of the heating (D) is set to $\pi/18$, or 10°. We set $p_0 = 550\,\mathrm{hPa}$ and $p_1 = 700\,\mathrm{hPa}$ to mimic the heating profile of tropical deep convection, in which heating is evident in the 200–900-hPa layer and maximizes roughly near the midtroposphere (e.g., Ling and Zhang 2013). Such an idealized heating profile is not necessarily perfect but could help estimate the flow responses to tropical precipitation (e.g., Yoo et al. 2012). The spatial configurations of the diabatic forcing are decided based on the RWBw-associated variations of seasonal mean precipitation, which will be further described in section 3. The diabatic forcing is applied throughout the integration of the idealized experiments. Since a constant source of heating or cooling can rapidly distort the mean temperature of the simulated atmosphere, we also include weak and horizontally homogeneous forcing between 25°S and 55°N to compensate any excessive heating or cooling.

Our extratropical perturbation experiment, which is similar to that in Franzke et al. (2004), examines how upstream atmospheric perturbations over the North Pacific and North America contribute to RWBw events. In addition to the basic-state flow, the experiment needs the input of initial perturbations. Instead of using linear regression of filtered data (Franzke et al. 2004), we derive initial perturbations by calculating composites of atmospheric anomalies associated with each weather regime (section 4). When initializing our simulations, we perturb the flow within the region where the weather regimes are defined. On the edges of the region, the initial state smoothly transitions to the July–October seasonal mean. We have run simulations for all the identified weather regimes, but our discussion will focus on the weather regimes that are most closely associated with RWBw events.

3. RWBw events and variability of tropical ocean and atmosphere

a. *Interannual variations associated with RWBw events*

We first examine the environmental variations associated with the interannual variations of RWBw events. Following Zhang et al. (2017), we select eight years with the highest and the lowest frequency of RWBw occurrence, respectively. We then build composites of the active [RWBw(+)] and the inactive [RWB(−)] phases and present their differences. The composite difference of SST (Fig. 1a) is consistent with Table 1 and suggests

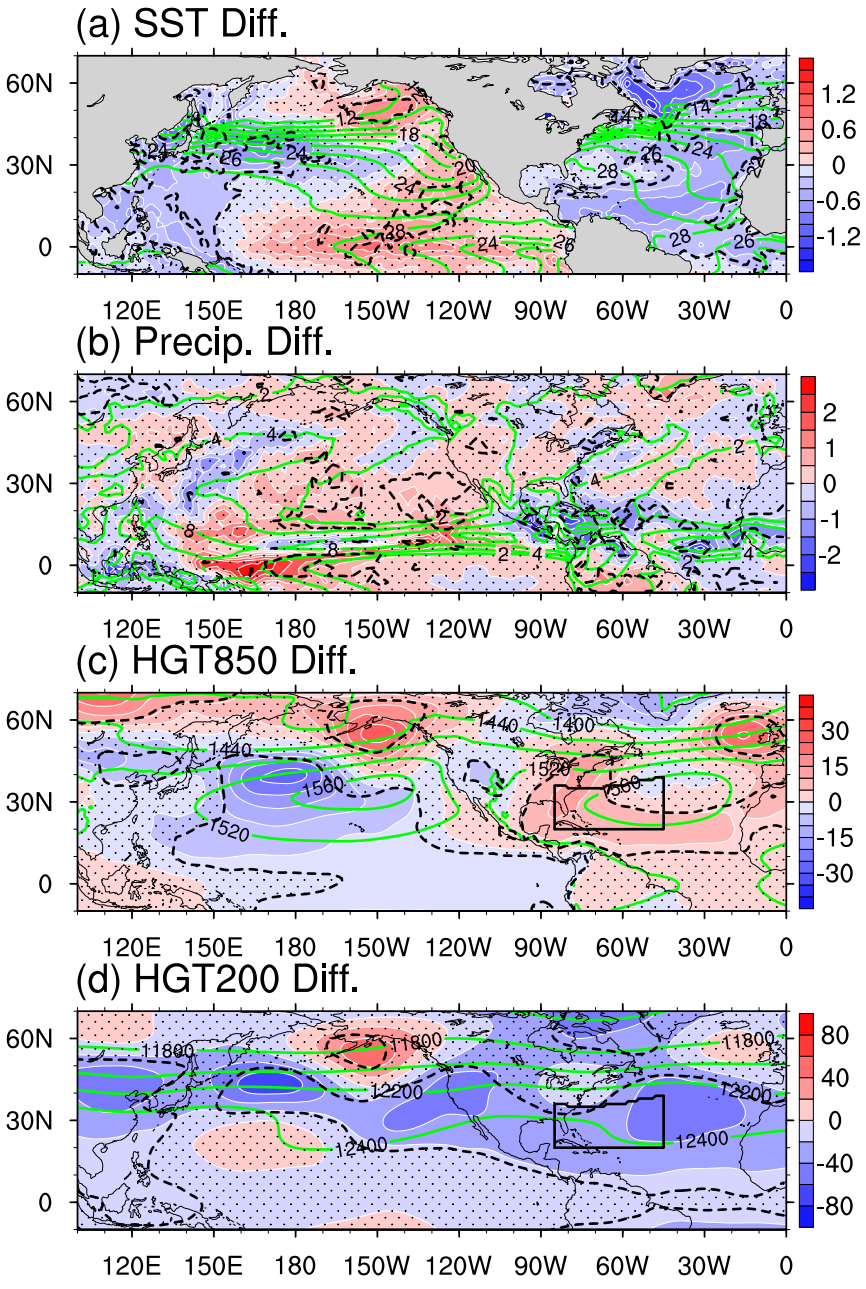

FIG. 1. Environmental variations related to interannual variations of the RWBw events. Two phases with extreme frequency of the RWBw occurrence, each of which includes 8 years, are used to build composite differences (color shading). The RWBw(+) phase includes 1983, 1984, 1985, 1986, 1990, 1993, 2002, and 2013, while the RWBw(−) phase includes 1988, 1995, 1998, 1999, 2005, 2006, 2008, and 2010. The composite differences are the composite means of years with more RWBw events minus the opposite. The analyzed variables include (a) SST (unit: °C), (b) PW (unit: mm day^{-1}), (c) 850-hPa geopotential height (unit: m), and (d) 200-hPa geopotential height (unit: m). The green contours show the 1981–2010 climatology. Black dashed lines highlight the parts above the 95% confidence level, which are free of stippling. The statistical significance is tested using the two-tailed Student's t test. The black solid lines in (c) and (d) denote the location of the high-PV tongues associated with the RWBw events.

that higher seasonal frequency of RWBw occurrence corresponds to lower SST of the North Atlantic. The RWBw-associated SST variations cover almost the entire basin and resemble the pattern of the Atlantic multidecadal variability (e.g., Goldenberg et al. 2001). The relatively strong SST anomalies over the tropical and midlatitude North Atlantic and the weak SST anomalies in between are reminiscent of the Atlantic horseshoe pattern (Czaja and Frankignoul 2002; Cassou et al. 2004). In addition, the tropical part of the variations in Fig. 1a resembles the Atlantic meridional mode during the hurricane season [Fig. 2 in Smirnov and Vimont (2011)]. In the Pacific basin, the SST pattern is similar to the combination of the Pacific meridional mode (e.g., Chiang and Vimont 2004) and the central Pacific El Niño (e.g., Kao and Yu 2009). The Pacific SST pattern is related to the development of El Niño events, which involves the propagation of subtropical SST anomalies to the equator (e.g., Alexander et al. 2010). In addition, the tropical SST anomalies in the Atlantic and the Pacific are also consistent with an interbasin teleconnection related to variations of the Walker circulation (Li et al. 2016), even though the correlations between the indices of Pacific SST and RWBw events are weak (Table 1).

The SST variations are accompanied by significant variations of tropical precipitation (Fig. 1b). The variations are pronounced in the Caribbean region (about $-2\,\mathrm{mm\,day^{-1}}$), and the magnitude of the Caribbean variations is comparable to that of the local long-term mean. The variations are consistent with earlier studies (e.g., Sutton and Hodson 2007; Smirnov and Vimont 2011), which suggest that the cooling of the North Atlantic, especially its tropical part, contributes to a reduction of precipitation near the Antilles. Precipitation variations are also evident across the tropical Pacific, especially near the equatorial regions of the central and eastern Pacific. Although the strongest variations ($>3\,\mathrm{mm\,day^{-1}}$) appears near 160°E, statistically significant variations mostly appear in the central and eastern parts of the basin.

Significant variations of the atmospheric circulation are present in both the tropics and the extratropics (Figs. 1c,d). In the North Atlantic basin, frequent RWBw events correspond to a stronger subtropical high that extends westward and southward (Fig. 1c). The lower-level variations are accompanied by a deeper midocean trough at the upper level (Fig. 1d) (e.g., Postel and Hitchman 1999; Zhang et al. 2016). In addition, significant geopotential height perturbations at the upper level extend westward and connect to the anomalies over the North Pacific between 20° and 50°N. Unlike the low-latitude perturbations, the perturbations over the extratropical North Pacific have a vertical structure that is nearly equivalent barotropic. The upper-level pattern of the North Pacific perturbations resembles a wave train that extends from the tropical western Pacific. Although the 200-hPa geopotential height variations do not reach the 95% confidence level over the subtropical northwestern Pacific, the signature of the subtropical node is statistically significant in the 200-hPa streamfunction field (not shown) and might be part of the basin-scale wave train. The wave train pattern resembles a preferred response of the summertime circulation that can be excited by tropical forcing at various longitudes across the Pacific and the eastern Indian Ocean (e.g., Fig. 11 in Lau and Peng 1992). The preferred response pattern is considered related to a normal mode of the summertime mean flow, which can also be excited by the internal variability of the extratropical flow (Lau and Peng 1992).

Overall, the composites are consistent with Table 1 and suggest that the seasonal variations of the RWBw events may have physical connections with the environmental changes related to climate modes. Some of the seasonal mean variations, such as the flow anomalies over the southeast of North America (Fig. 1c) and the North Pacific (Fig. 1d), appear in regions where the synoptic precursors of RWBw events develop (Zhang and Wang 2018). The variations of the basic-state flow could potentially affect behaviors of Rossby waves and thus the frequency of RWBw occurrence. For example, the 200-hPa flow variations near the Gulf of Alaska, as suggested by wintertime studies (e.g., Drouard et al. 2015), might modulate the wave propagation from the North Pacific to the North Atlantic, as well as the wave orientation and the ensuing breaking over the North Atlantic. To understand the potential tropical–extratropical interaction, it is necessary to explore whether the basic-state flow variations are associated with the tropical forcing in Fig. 1. In the following section, we will explore how the precipitation of the Caribbean and the central Pacific may affect the large-scale circulation and RWBw events.

b. Tropical precipitation forcing and RWBw events: Idealized model simulations

To investigate the flow responses to the variations of tropical precipitation (Fig. 1), we apply an idealized thermodynamic forcing in regions of interest (Fig. 2). The discussion will focus on experiments driven by the thermodynamic forcing associated with the RWBw(+) phase. Using the forcing associated with the RWB(−) phase produces similar responses with the opposite signs. Here we describe the results from three experiment settings: 1) the precipitation deficit at the Caribbean

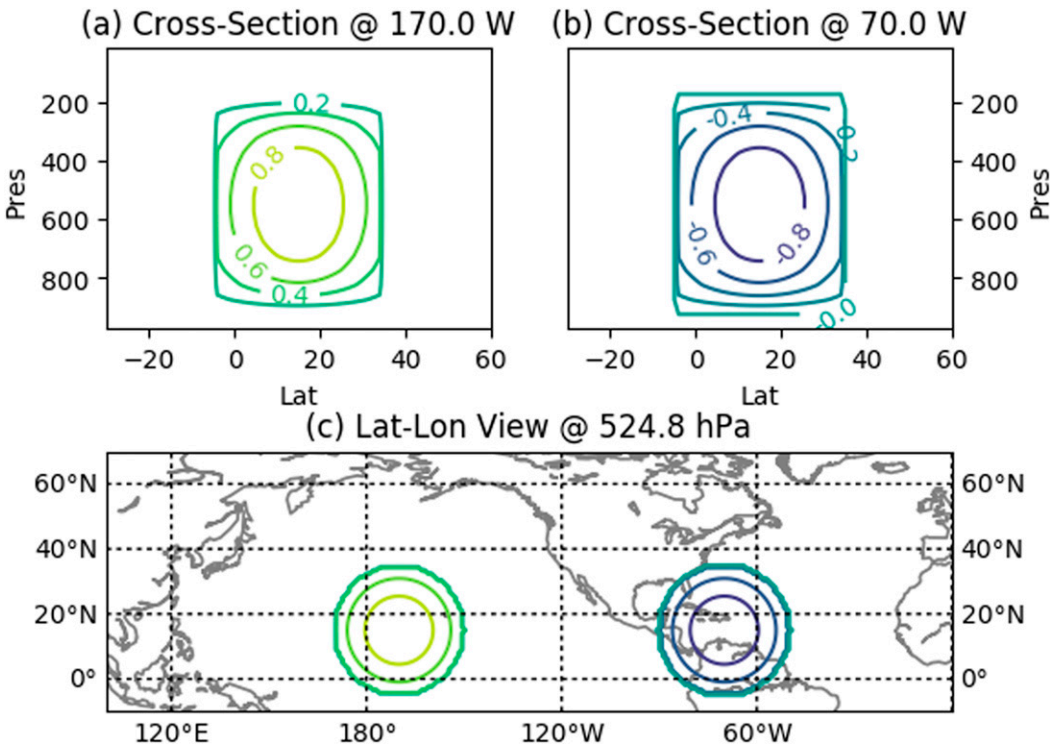

FIG. 2. Idealized forcing (CAR_Neg + CP_Pos). The unit is K day^{-1}, and the maximum intensity of the heating and the cooling is 1 K day^{-1}, approximately corresponding to the interannual variations of precipitation (Fig. 1b). The horizontal and vertical axes of (a) and (b) show latitudes (unit: degrees north) and pressure level (unit: hPa), respectively.

(CAR_Neg), with the cooling centering at 15°N, 70°W; 2) the precipitation surplus at the central Pacific (CP_Pos), with the heating centering at 15°N, 170°W; and 3) the combination of the former two (CAR_Neg + CP_Pos). The forcing location is specified to mimic the locations of the significant tropical precipitation anomalies close to the subtropical westerlies, where the background vorticity and its gradient are larger. Such an environment helps diabatic heating to generate stronger Rossby wave sources and flow responses (Sardeshmukh and Hoskins 1988). Consistently, sensitivity tests suggest that the heating variations at the equatorial central Pacific (near 0°N, 170°W) and the eastern Pacific (near 10°N, 130°W) have relatively weak impacts on the extratropics of the Northern Hemisphere (not shown).

The model integrations suggest that the flow responses in the subtropics are quasi-stationary, and the peripheral extratropical responses extend eastward and slowly evolve (not shown). By day 20 of the integration, the extratropical flow responses have almost circled the globe and started to amplify rapidly along the subtropical jet over the Asia. The amplified perturbations soon reach the North Pacific and complicate the flow pattern. Even though the flow responses at lower latitudes can remain steady (Rodwell and Hoskins 2001), the extratropical flow responses by that time likely have been undermined by nonlinear artifacts, which are related to the forcing term that is specified to keep the basic-state flow steady. The nonlinear artifacts start to become comparable to flow perturbations around 20 days after the model initialization (Franzke et al. 2004). To avoid the complexity, we mainly discuss the flow responses at day 18.

The idealized simulations suggest that the precipitation variations at both the Caribbean and the central Pacific affect the atmospheric circulation in the Northern Hemisphere (Fig. 3). Overall, the simulated circulation responses and the observation show better agreement in the subtropics than in the extratropics. Since the leading-order physics like the thermodynamic balance also differs across latitudes (Rodwell and Hoskins 2001), the subtropical and the extratropical circulation responses will be discussed separately.

The simulated *subtropical* responses to the CAR_Neg (Figs. 3a,b) and the CP_Pos forcing (Figs. 3c,d) are baroclinic and extend over broad regions. Both forcings help the Atlantic subtropical high and upper-tropospheric trough extend westward near the coast of

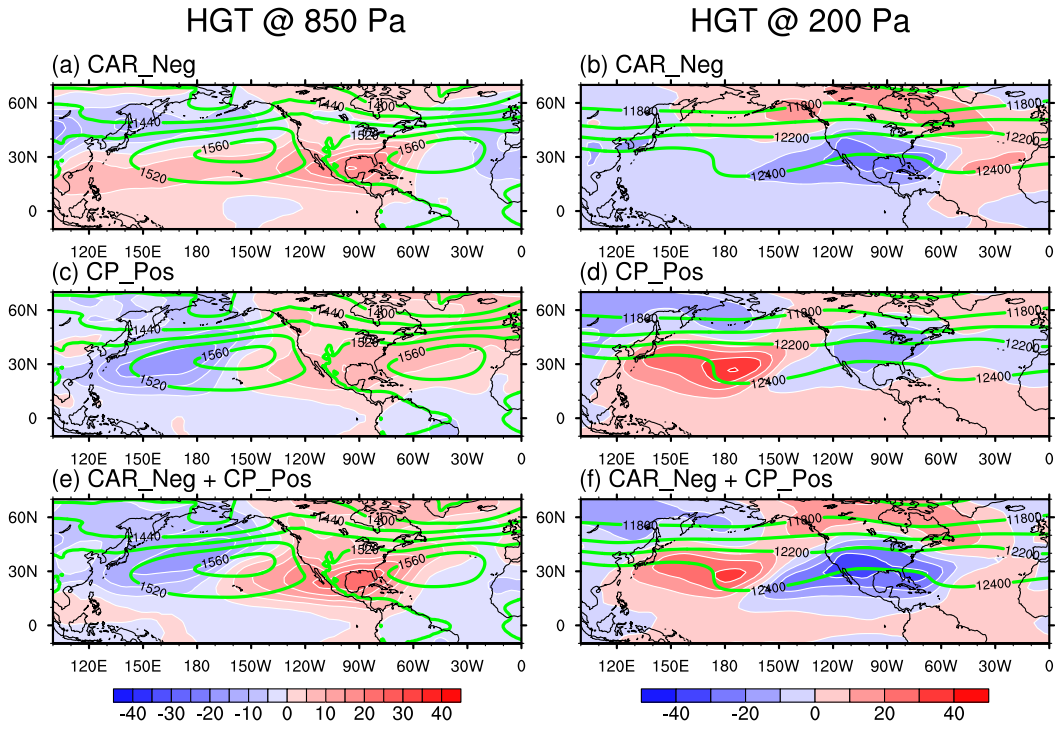

FIG. 3. Atmospheric flow responses to prescribed diabatic heating. Anomalies of (left) 850-hPa and (right) 200-hPa geopotential height (in m) in response to (a),(b) the CAR_Neg forcing, (c),(d) the CP_Pos forcing, and (e),(f) the CAR_Neg + CP_Pos forcing. Note that the shading settings differ from those in Figs. 1e and 1f. The green contours show the 1981–2010 climatology.

North America. The sum of the flow responses (Figs. 3e,f) resembles the observed variations over the Caribbean and the southeast United States (Fig. 1). The similarity is also evident in a cross section of the zonal flow averaged between 60° and 90°W (Fig. 4), where Rossby waves sometimes amplify quickly before breaking (Zhang and Wang 2018). The observation suggests that the midlatitude and the subtropical upper-level westerlies separate from each other when the RWBw events occur more frequently. On the equatorward flank of the midlatitude jet (30°–45°N), the negative responses to the CAR_Neg forcing (Fig. 4b) prevail over the positive responses to the CP_Pos forcing (Fig. 4c) and agree with the observed changes reasonably well. The subtropical flow responses are likely related to the Rossby wave responses to the CAR_Neg forcing (Sardeshmukh and Hoskins 1988). The flow deceleration near 35°N, along with the acceleration near 55°N that is not captured by the idealized model (Figs. 4a,d), increases the meridional shear of the zonal flow ($\partial u/\partial y$) on the equatorward flank of the midlatitude jet. As suggested by modeling studies (Thorncroft et al. 1993; Hartmann and Zuercher 1998), the flow configuration with relatively high anticyclonic shear favors the anticyclonic RWB behavior of baroclinic waves. Notably, the relation is consistent with the phasing relation in Fig. 1b, which suggests that less precipitation over the Caribbean corresponds to more RWBw events. The relation between the subtropical flow and the RWBw events can also be deduced via the critical layer argument (Randel and Held 1991), and a more detailed discussion is provided in section 5.

The simulated *extratropical* responses are generally weak and sometimes disagree with the observed variations. For example, the 200-hPa flow responses to the CAR_Neg + CP_Pos forcing (Fig. 3f) are a fraction of the observed variations near the Bering Sea, and show a sign that is opposite to the observation near the Hudson Bay. The disagreement is potentially related to our idealized model settings, which use idealized forcing sources and exclude moist diabatic processes that may amplify wave responses. In addition, the short integration time could inhibit the wave–flow interactions that regulate the variations of the midlatitude jet (e.g., Rivière 2009). The lack of such wave–flow interactions may help explain why the idealized experiments do not produce the observed displacement of the midlatitude jet (Figs. 4a,d). Finally, some full-physics ensemble simulations suggest that extratropical responses to the tropical SST forcing during the warm season are weak (Cassou et al. 2004; Sutton and Hodson 2007). We

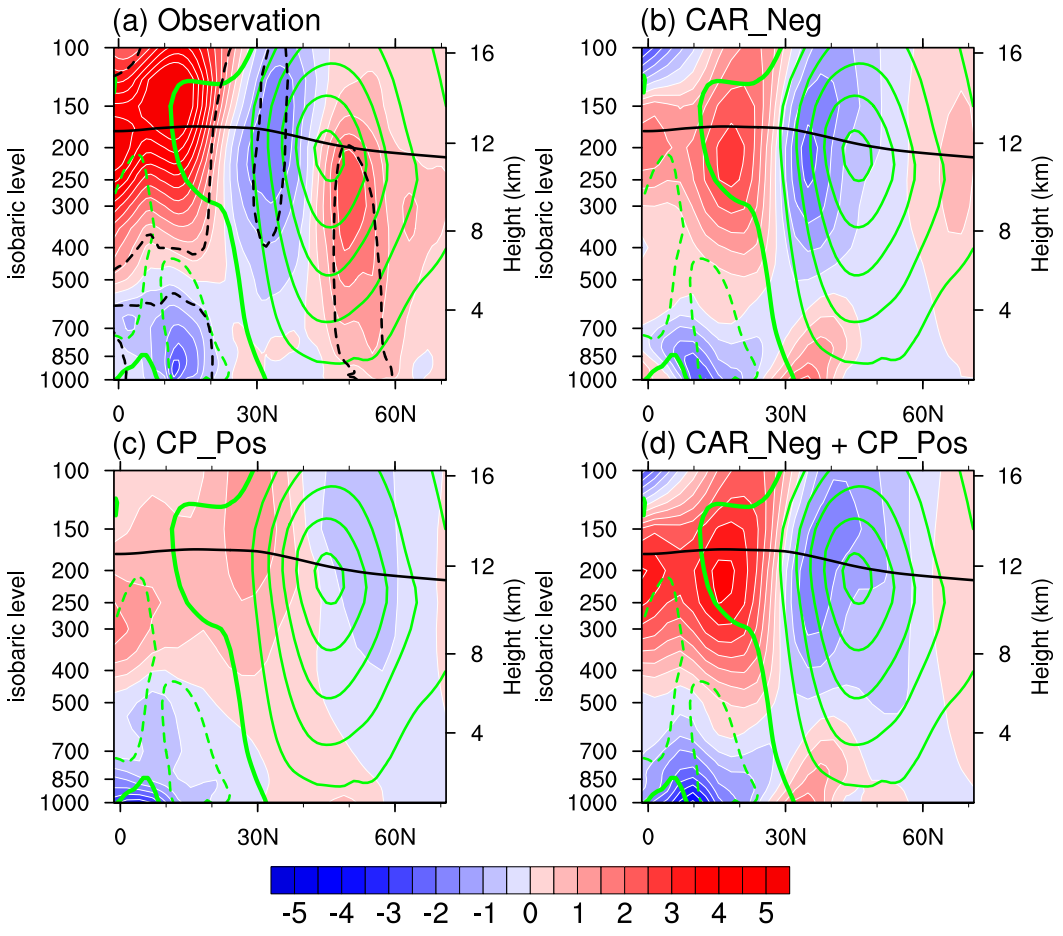

FIG. 4. Latitude–pressure cross section of zonal wind (shading, unit: m s^{-1}) averaged between 60° and 90°W. (a) Observed variations, the composite means of years with more RWBw events [RWBw(+)] minus the opposite [RWBw(−)], (b) responses to the CAR_Neg forcing, (c) responses to the CP_Pos forcing, and (d) responses to the CAR_Neg + CP_Pos forcing. The green contours show the 1981–2010 climatology. The solid green contours show positive values, and the dashed green contours show negative values. The thickened green contours show the zero value, and the contour intervals are 5 m s^{-1}. The black dashed contours in (a) highlight the values above the 95% confidence level. The black solid contours denote the 350-K isentropic surface.

speculate that the unforced variability, in addition to forcing from other regions, may also contribute to the observed flow variations in the extratropics (Figs. 1c,d).

c. *Response of tropical environment to RWBw events*

This section investigates how RWBw events may affect the tropical SST. Earlier studies have shown that the equatorward-propagating Rossby waves can actively affect tropical circulation (e.g., Walker and Schneider 2006) and tropical precipitation (e.g., Kiladis and Weickmann 1992; Kiladis 1998; Funatsu and Waugh 2008). The atmospheric variations associated with RWB during the Atlantic hurricane season have been documented in our companion studies (Zhang et al. 2017; Li et al. 2018; Zhang and Wang 2018), as well as in Papin (2017). Here we will focus on the possible impact of the RWBw events on the tropical SST, which is widely considered as a primary source of seasonal predictability of Atlantic TC activity.

Following Zhang et al. (2017), we identify RWBw events and build composites of the surface turbulent heat flux and the radiative heat flux from the ERA-Interim reanalysis. The turbulent heat flux consists of the latent and the sensible heat flux, and the radiative heat flux consists of the longwave and the shortwave radiation. When calculating flux anomalies, we removed the climatological seasonal cycle and the seasonal mean. The composite anomalies are presented in a relative coordinate system, the center of which corresponds to the centroid of the high-PV tongues (Fig. 5). For the convenience of the later discussion of SST anomalies, the heat fluxes that warm the ocean are designated

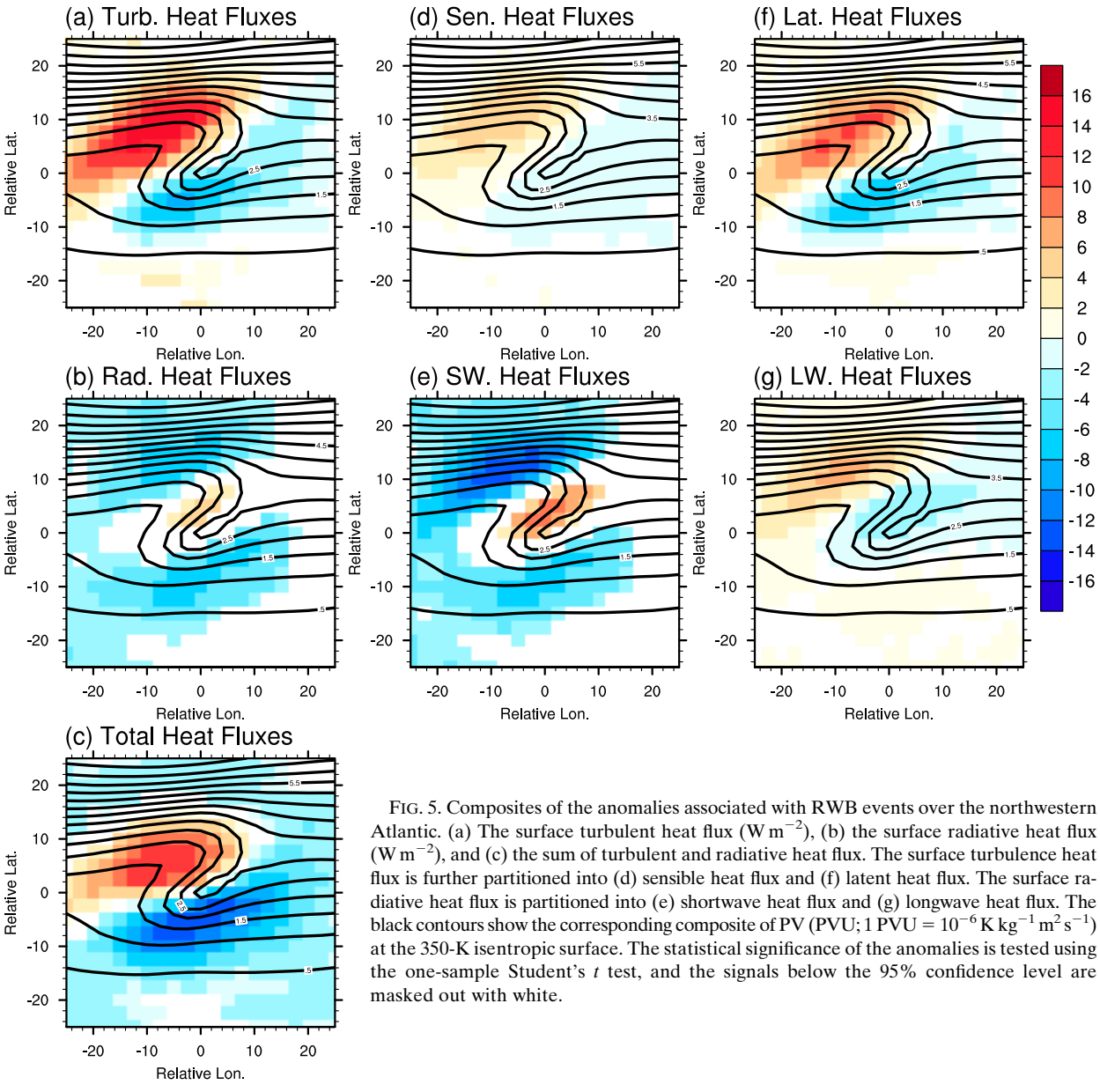

FIG. 5. Composites of the anomalies associated with RWB events over the northwestern Atlantic. (a) The surface turbulent heat flux ($W\,m^{-2}$), (b) the surface radiative heat flux ($W\,m^{-2}$), and (c) the sum of turbulent and radiative heat flux. The surface turbulence heat flux is further partitioned into (d) sensible heat flux and (f) latent heat flux. The surface radiative heat flux is partitioned into (e) shortwave heat flux and (g) longwave heat flux. The black contours show the corresponding composite of PV (PVU; $1\,PVU = 10^{-6}\,K\,kg^{-1}\,m^2\,s^{-1}$) at the 350-K isentropic surface. The statistical significance of the anomalies is tested using the one-sample Student's t test, and the signals below the 95% confidence level are masked out with white.

with a positive sign. Before discussing the results, we note that the ERA-Interim flux data, like the other data products of surface fluxes, are subject to the uncertainties related to model errors and the lack of reliable in situ observations (Brunke et al. 2011). For example, the uncertainties of the turbulent heat flux reported by Brunke et al. (2011) and the anomalies to be examined are on the same order. Therefore, our discussion of the surface fluxes will emphasize the qualitative aspects and the most coherent patterns.

The anomalies of the turbulent heat flux (Fig. 5a) show a dipole pattern near the breaking wave. The dipole pattern of anomalous turbulent heat fluxes is consistent with those of the RWB events in the Pacific basin (Strong and Magnusdottir 2009) and arise from near-surface airstreams of distinct properties. For example, the strongest positive anomalies (about $14\,W\,m^{-2}$) appear in the northwestern sector of the breaking wave, where the low-level flow contributes to the poleward advection of the warm and humid air (Zhang et al. 2017). The southwesterly anomalies strengthen the climatological southwesterly near the eastern coast of North America, which can be inferred from the 850-hPa geopotential height field (Fig. 1c). Meanwhile, the warm and humid airstream reduces the thermodynamic disequilibria at the air–sea interface, which are typically

large over the warm Gulf Stream (not shown). Although both the wind speed and the thermodynamic disequilibria can affect the surface heat fluxes (e.g., Brunke et al. 2011), the reduction of the interface disequilibria prevails near the east coast of North America and suppresses the transfer of heat from the ocean to the atmosphere. Consequently, the east coast of North America is dominated by positive anomalies of turbulent heat flux, indicating anomalous warming of the ocean (Figs. 5a,d,f).

The anomalies of the radiative heat flux (Fig. 5b) show a pattern of tripoles that are aligned meridionally. The tripole pattern features weak positive anomalies near the domain center and stronger negative anomalies on the northern and southern flanks. The anomalies of the radiative flux are dominated by the shortwave radiation (Fig. 5e) and involve variations of moisture distribution and cloud cover. For example, the negative anomalies are mainly related to an increase of cloud amount in the overlying atmosphere (not shown), which tends to reduce the amount of shortwave radiation that reaches the surface. Those cloud variations are coupled with anomalies of vertical motion and humidity associated with wave breaking (Figs. 4 and 5 in Zhang et al. 2017). But given the uncertainty of the cloud representation in the reanalysis dataset, we refrain from further discussing the quantitative aspects of the cloud influence on the radiative heat flux.

The contributions by the turbulent and the radiative heat flux to the overall heat exchange vary spatially (Figs. 5a–c). In the northern part of the domain, the anomalies of the radiative flux (Fig. 5b) are generally weaker than the anomalies of the turbulent heat flux (Fig. 5a). However, the former becomes comparable to the latter in the southern part of the relative coordinate system, which corresponds to the subtropical and tropical North Atlantic. One should thus examine both the turbulent and the radiative heat fluxes when evaluating the impact of RWB events on the underlying ocean.

We now examine how the surface flux anomalies affect the SST of the North Atlantic. Instead of continuing with the relative coordinate system, we build composites in the native latitude–longitude coordinate system to better illustrate how the anomalies project on the large-scale SST pattern. This choice leads to some spatial misalignment of the RWB-associated anomalies, which tends to weaken RWB-associated signatures. To mitigate the issue, we select the RWBw events that appear in a narrower longitudinal range (50°–75°W instead of 45°–85°W). In addition, we focus on the RWBw events with extensive high-PV tongues at the 350-K isentropic surface. Such events tend to accompany with stronger near-surface anomalies (Papin 2017). We select such events using an area index of the RWB-associated high-PV tongues, which is defined as the area covered by the high-PV tongues and calculated at a 6-hourly interval (Zhang and Wang 2018). After removing the climatological seasonal cycle and the seasonal means of individual years from the area index, we select time steps when the area index deviates from zero by at least one standard deviation. The RWBw events that meet the criteria add up to 2569 and correspond to about 73 (or 15%) time steps of each season.

We examine the selected subset of RWBw events and show the composite anomalies of the surface heat flux, the 10-m wind, and the SST with no time lag (Fig. 6a). The anomalous surface heat flux shows a horseshoe-like pattern in the North Atlantic. The significant positive anomalies near the east coast of North America reach a strength of $>15\,\mathrm{W\,m^{-2}}$ and are mainly contributed by the turbulent heat flux (not shown). The positive anomalies, as suggested in the discussion of Fig. 5a, arise from the reduced interface disequilibria that are associated with the poleward airstreams. In addition to the positive anomalies of surface heat flux, the significant negative anomalies reach $<-10\,\mathrm{W\,m^{-2}}$ east of the Labrador Sea and $<-15\,\mathrm{W\,m^{-2}}$ near the Greater Antilles, respectively. Consistent with Fig. 5, the negative flux anomalies near the Greater Antilles see comparable contributions from the turbulent heat flux and the radiative heat flux (not shown). On the basin scale, extensive anomalies of the surface heat flux are accompanied by significant SST anomalies that show a similar spatial pattern. In addition, the signs of flux and SST anomalies suggest that the atmospheric perturbations actively contribute to the SST anomalies. The attribution is supported by an examination of the SST evolution, which suggests that the SST anomalies in Fig. 6a mostly build up within a 4-day period prior to wave breaking (Fig. 6b) and persist at least 4 days afterward (Fig. 6c).

The magnitude of the SST anomalies associated with individual RWB events is weak, but their accumulative impact could be substantial. For example, the SST anomalies in the tropical North Atlantic can reach $-0.04\,\mathrm{K}$ (Fig. 6). However, the RWBw events on average occur at about 73 six-hourly time steps per season, with a standard deviation of about 21 time steps per season. Therefore, the standard deviation implies that interannual variations of the RWBw events correspond to an accumulative tendency of SST of about 0.8 K per season, which is comparable to the interannual variations of SST in the tropical North Atlantic (Fig. 1a). The value here only serves as a crude estimate, and two caveats should be noted. First, some of those RWB events occur within the same RWB episode, and the SST anomalies in Fig. 6 may be cumulative. Second, the

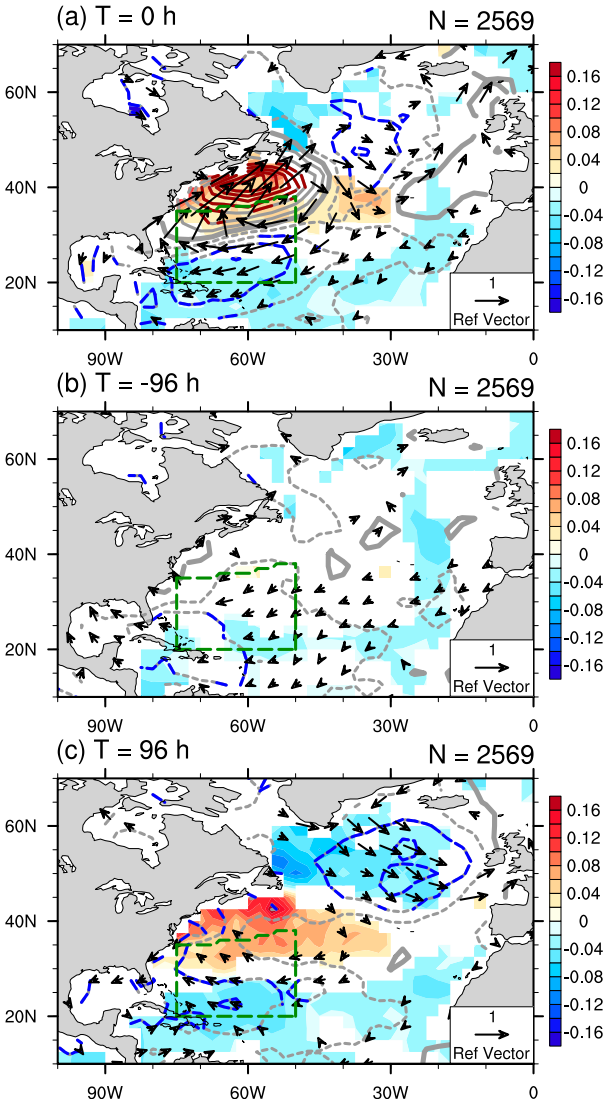

FIG. 6. (a) Impacts of selected Atlantic RWB events on the SST (no time lag). The gray contours show the anomalies of the surface heat flux (turbulent + radiative), the color shading shows the anomalies of SST, and the vectors show the anomalies of the wind that is 10 m above the surface. The units are W m^{-2}, K, and m s^{-1}, respectively. The contour intervals of the heat flux anomalies are 5 W m^{-2}, and the heat flux that warms the ocean is designated with the positive sign. We show the positive values with solid lines and negative values with dashed lines. The thick solid lines denote the zero contours. The flux anomalies above the 90% confidence level are highlighted with red and blue lines. The SST and wind anomalies that are below the 90% confidence level are masked out. The statistical significance of the anomalies is tested using the one-sample Student's *t* test. The green dashed lines denote the location of the high-PV tongues associated with the RWB events that are used in the composites. (b),(c) As in (a), but for 96 h before and after the selected RWB events, respectively.

calculation does not consider the heat transfer from the surface to the ocean mixed layer and may overestimate the seasonal-scale response of the upper ocean. Despite those limitations, the consistent horseshoe patterns of SST variations on both synoptic (Fig. 6) and seasonal (Fig. 1a) scales support that RWBw events may contribute to seasonal variations of North Atlantic SST.

Given that the SST-regulated tropical precipitation can modulate the basic-state atmosphere flow (section 3b) and potentially the frequency of RWBw occurrence (more in section 4c), the analysis here suggests a possible interaction between RWBw events and variations of tropical SST. One possible loop is as follows: negative anomalies of the tropical North Atlantic SST suppress the Caribbean precipitation and contribute to anomalies of the basic-state flow, such as an increase of the upper-level anticyclonic shear near the midlatitude jet and a displacement of the critical layer. The basic-state flow changes then facilitate RWB events over the northwestern Atlantic, which in turn affect the tropical atmosphere and enhance or sustain the tropical SST anomalies. Such an interaction likely operates with opposite anomalies and may help explain the negative strong correlation between the seasonal frequency of the RWBw occurrence and the SST of the tropical North Atlantic (Table 1). We do not rule out the possibility that the interaction involves additional physical mechanisms. For example, the SST variations can modulate the low-level baroclinicity in the subtropics. Despite the relatively weak atmospheric baroclinicity during the warm season, the negative anomalies of the tropical North Atlantic SST might still reduce the low-level baroclinicity significantly and favor anticyclonic RWB via the mechanisms described by Orlanski (2003) and Rivière (2009, 2011).

Nonetheless, we caution that the proposed RWB–SST interaction does not fully explain the variations of tropical SST or the RWBw events. For example, the mixed layer of the tropical ocean has large thermal inertia, so tropical SST during the hurricane season is strongly influenced by anomalies that are present before the season [Fig. 8 in Chen and Lin (2013)]. Additionally, much variability of the extratropical atmosphere (Sutton and Hodson 2007; Coumou et al. 2015; Vavrus et al. 2017) is not driven by tropical SST forcing, and these unforced extratropical variations likely also affect variations of RWBw events. In the next section, we will examine extratropical atmosphere variability and its association with the RWBw events.

4. RWBw events and variability of extratropical atmosphere

a. *Weather regimes and RWBw events: Observational analysis*

We first examine the variability of the extratropical circulation in the North Atlantic domain using the

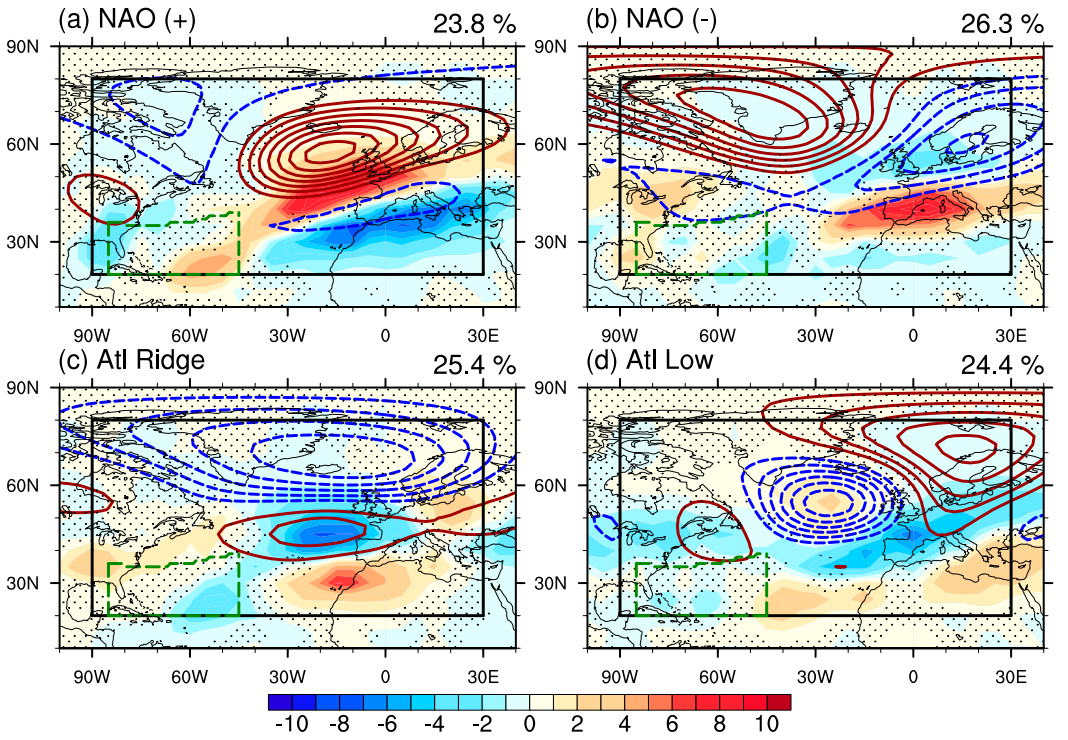

FIG. 7. Weather regimes and the associated variations of RWB events in the domain of North Atlantic (20°–80°N, 90°W–30°E; denoted with black solid lines). The contours show the anomalies of 200-hPa geopotential height, and the color shading shows the variations of RWB occurrences on the 350-K isentropic surface. The contour intervals of geopotential height anomalies are 20 m. The positive values are plotted with the red solid lines, and the negative values are plotted with the blue dashed lines. The zero contours are omitted for clarity. The unit of RWB occurrence is events per season. The RWB variations that fail to pass the 90% confidence level are masked with black dots. The green dashed lines denote the location of the high-PV tongues associated with the RWBw events.

weather regime analysis (Fig. 7). The analysis follows earlier studies and is conducted at the 500-hPa level, which is also representative of the upper troposphere. We mainly discuss the regime-related anomalies at the 200-hPa level to better illustrate the connection between weather perturbations and the RWBw events. We categorize the 6-hourly geopotential height anomalies into four types and refer them to as NAO(+), NAO(−), Atlantic ridge, and Atlantic low, respectively. The naming follows Cassou et al. (2005) except that we refer to their ''blocking'' pattern as NAO(+) given that the pattern is roughly opposite to the NAO(−) pattern and resembles the NAO(+) pattern in Folland et al. (2009). The occurrence frequency of each weather regime is about 25% during July–October of 1979–2013. Given our interest in clarifying the NAO–TC relation, we primarily discuss the NAO(+) and NAO(−) regimes. Their strongest geopotential height anomalies appear in the extratropics and are accompanied by significant anomalies of anticyclonic RWB. For example, the NAO(+) regime features a displacement of RWB occurrences from about 35°N to about 45°N over the east Atlantic and Europe, as well as ridging to the northwest of breaking waves (Fig. 7a). Ridging like this contributes to the reversal of PV contours by advecting low-PV air poleward and high-PV air equatorward, making it a salient feature of anticyclonic RWB (e.g., Postel and Hitchman 1999; Abatzoglou and Magnusdottir 2006). Overall, the result underscores the physical connection between RWB and weather regimes (e.g., Michel and Rivière 2011; Swenson and Straus 2017).

The spatial relation between the RWB events and weather regimes sheds light on the NAO–TC relation. The two NAO regimes are closely associated with RWB events in the east Atlantic, which have relatively weak impacts on the basinwide TC activity (Zhang et al. 2017). In contrast, the NAO regimes show only weak connections with the RWBw events, which have greater influences on Atlantic TC activity (Zhang et al. 2017). Admittedly, there are statistically significant anomalies within the RWBw domain (Figs. 7a,b), but the anomalies of different signs tend to cancel out when we consider the total count of the RWBw events (i.e., the RWBw index in Table 1). Overall, the evidence indicates that the

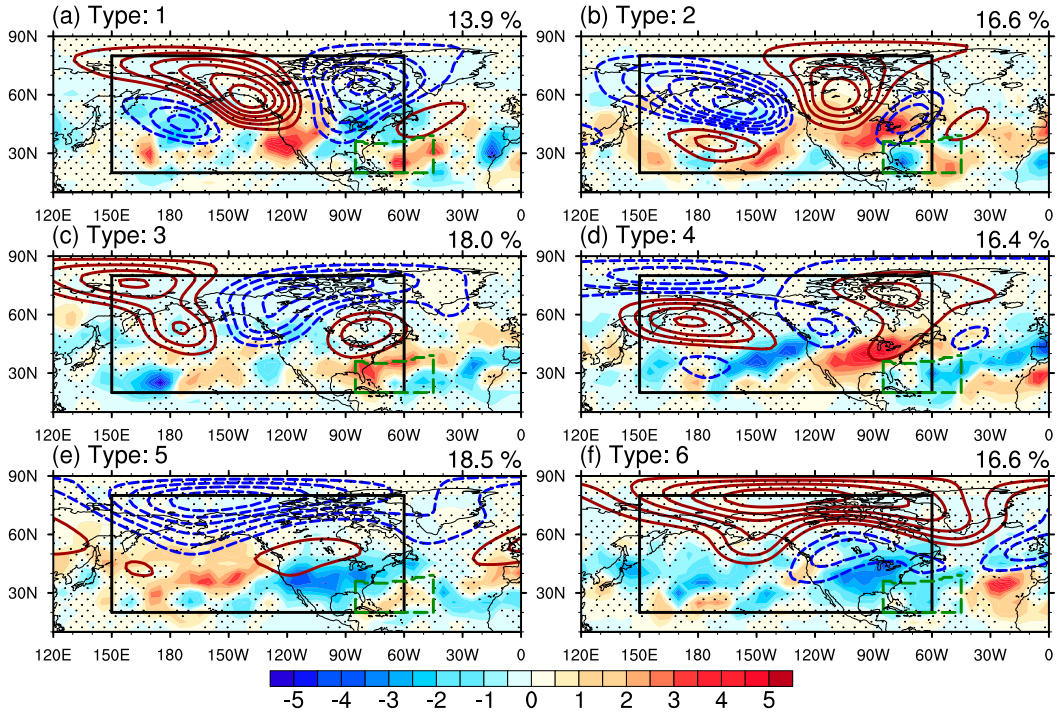

FIG. 8. As in Fig. 7, but for the domain of North Pacific and North America (20°–80°N, 150°E–60°W). The variations of RWB occurrences lag the weather regimes by 5 days.

NAO regimes can affect TC activity but only to a limited extent. This finding, in addition to the diverse indices (e.g., Barnston and Livezey 1987; Jones et al. 1997; Folland et al. 2009) that have been used to characterize the summertime NAO, helps explain why a large body of past studies drew inconsistent conclusions about the NAO–TC relation.

Similar to the NAO regimes, the Atlantic ridge and the Atlantic low regimes show patchy and/or weak anomalies of RWB counts over the northwestern subtropical Atlantic (Fig. 7). Therefore, none of the Atlantic weather regimes are closely associated with the RWBw events. What else may affect variations of RWBw events? Our earlier study of the wave life cycle suggests influences from the upstream flow (Zhang and Wang 2018). More specifically, the Rossby waves that break near the east coast of North America can be traced back to the North Pacific. In addition, wintertime studies also suggest that characteristics of upstream perturbations and basic-state flow can affect RWB in the North Atlantic basin (e.g., Benedict et al. 2004; Franzke et al. 2004; Drouard et al. 2015). These findings motivate us to examine variations of the upstream flow and its relation with the RWBw events.

In the North Pacific–North America domain (section 2b), we categorize the 6-hourly geopotential height anomalies into six regimes (Fig. 8). The frequency of occurrence of each weather regime is about 16%. The magnitude of the 200-hPa geopotential height anomalies can reach >100 m, which is about twice as strong as the interannual variations of the seasonal mean field (Fig. 1d). Type 1 (Fig. 8a) and type 2 (Fig. 8b) show wave train patterns that span from the North Pacific to the North Atlantic. Especially, the wave train pattern of type 1 resembles the synoptic-scale pattern that precedes RWBw events (Zhang and Wang 2018). In addition, the activity centers of the wave train are aligned with those of the wave train in Fig. 1d, suggesting the synoptic perturbations could project onto the seasonal pattern. Type 3 (Fig. 8c) and type 4 (Fig. 8d) show complex patterns at both high latitudes and midlatitudes, which are possibly manifestations of atmospheric blocking and may indicate connections between the midlatitude and the Arctic weather. Type 5 (Fig. 8e) and type 6 (Fig. 8f) are nearly opposite patterns that feature an activity center in the Arctic region of North America. When viewed in a larger domain (not shown), the regimes have another activity center in the Eurasian sector of the Arctic region. Such patterns resemble the two phases of the Arctic dipole pattern, which contributes to variations of the Arctic sea ice (e.g., Wang et al. 2009). The seasonal counts of the six weather regimes are not significantly correlated with the indices of the Pacific–North America pattern or the Arctic Oscillation

(not shown), possibly because the two patterns are less robust during the warm season (e.g., Barnston and Livezey 1987).

All the six weather regimes in Fig. 8 are accompanied by significant distribution variations of anticyclonic RWB events. The variations are generally pronounced within the band of 25°–50°N in a few action centers, such as the northeastern Pacific and North America. In particular, the RWB events over North America are associated with multiple weather regimes and significant variations of meteorological variables (e.g., surface temperature; not shown), which are likely related to some extreme weather events (Bosart et al. 2017). But given that Atlantic TC activity motivates the study, the following discussion will focus on the regimes can clearly lead to the RWBw events, namely types 1 and 3. We will investigate the regime–RWB relation and the underlying physical mechanism using idealized simulations.

b. *Weather regimes and RWBw events: Idealized model simulations*

To further illustrate the physical connection between the upstream weather regimes and the ensuing RWB events, we investigate the evolution of type 1 and type 3 regimes using idealized simulations. As discussed in section 2c the perturbations associated with the two weather regimes are added to the basic-state flow as the initial condition. During the ensuing model integrations, the agreement between the simulated flow state and the observed flow state gradually degrades (not shown). Nonetheless, their agreement is acceptable within the first 5 days, and we will primarily discuss simulation results from that period. When evaluating the flow evolution, we use the wave activity flux (Takaya and Nakamura 2001) that points approximately in the direction of wave energy propagation. Specially, a convergence of equatorward wave activity flux is consistent with anticyclonic RWB (Magnusdottir and Haynes 1996).

The evolution of type 1 regime suggests an eastward propagation of Rossby waves (Figs. 9a–c). At day 1, the wave activity flux suggests that the wave propagates from the North Pacific to the North Atlantic. In the following four days, the energy dispersion weakens the geopotential height anomalies over the North Pacific by about 50% but helps maintain the downstream activity centers. Near the ridge node over the North Atlantic, the wave activity flux suggests an equatorward propagation of the Rossby wave, which is often associated with anticyclonic RWB (Thorncroft et al. 1993; Magnusdottir and Haynes 1996; Drouard et al. 2015). The equatorward propagation, the geopotential height anomalies, and the PV pattern are consistent with RWB signatures in Fig. 8a. Overall, the simulated wave evolution is consistent with the wave evolution examined by Zhang and Wang (2018) despite some differences. For example, the ridge node over the western North Atlantic does not show a rapid amplification, which is associated with diabatic processes (Zhang and Wang 2018) and thus unlikely captured by a dry idealized model. Nonetheless, the differences do not undermine the finding that the type 1 regime can contribute to the RWBw events.

The evolution of the type 3 regime also features a downstream energy dispersion and the ridging signature of wave breaking (Figs. 9d–f). At day 1, the anomalies of geopotential height are pronounced near the Bering Strait and over North America. In the following four days, the wave activity flux suggests a dispersion of wave energy from the high latitudes to the subtropics near the western North Atlantic. The flux helps maintain the ridge anomaly over North America, which persists about 7 days in our idealized simulation (not shown). The ridge anomaly resides on the northern flank of the climatological midlatitude jet and resembles the cutoff high pattern, which occasionally appears during the summertime as a block pattern (Tyrlis and Hoskins 2008) and contributes to warm moist weather near the east coast of North America. Although the wave activity flux is consistent with the elevated activity of anticyclonic RWB over the northwestern Atlantic (Fig. 8c), the simulated PV does not show a contour reversal. The lack of the RWB pattern suggests that the moist diabatic processes, which are absent in the dry idealized model, may be essential for the RWB events associated with the type 3 regime.

Overall, the analyses and simulations in sections 4a and 4b indicate that variations of the upstream flow correspond to the variations of RWB events on the intraseasonal scale. At least two weather regimes, namely type 1 and type 3 in the North Pacific–North America domain, channel Rossby waves from higher latitudes and favor anticyclonic RWB in the subtropics. Consistent with wintertime studies (e.g., Drouard et al. 2013, 2015), the upstream modulation contributes to variations of the RWBw events on the synoptic to intraseasonal scale. However, we note that the correlations between the seasonal counts of the RWBw events and the weather regimes do not reach the 90% confidence level on the interannual time scale (not shown). The interannual correlations may suffer from the seasonal averaging, which may allow the relation between a specific weather regime and the RWBw events to be blurred by signatures related to other regimes. The interannual associations may also be obscured by tropical climate modes, which can affect the basic-state flow (section 3b) and potentially the evolution and statistics

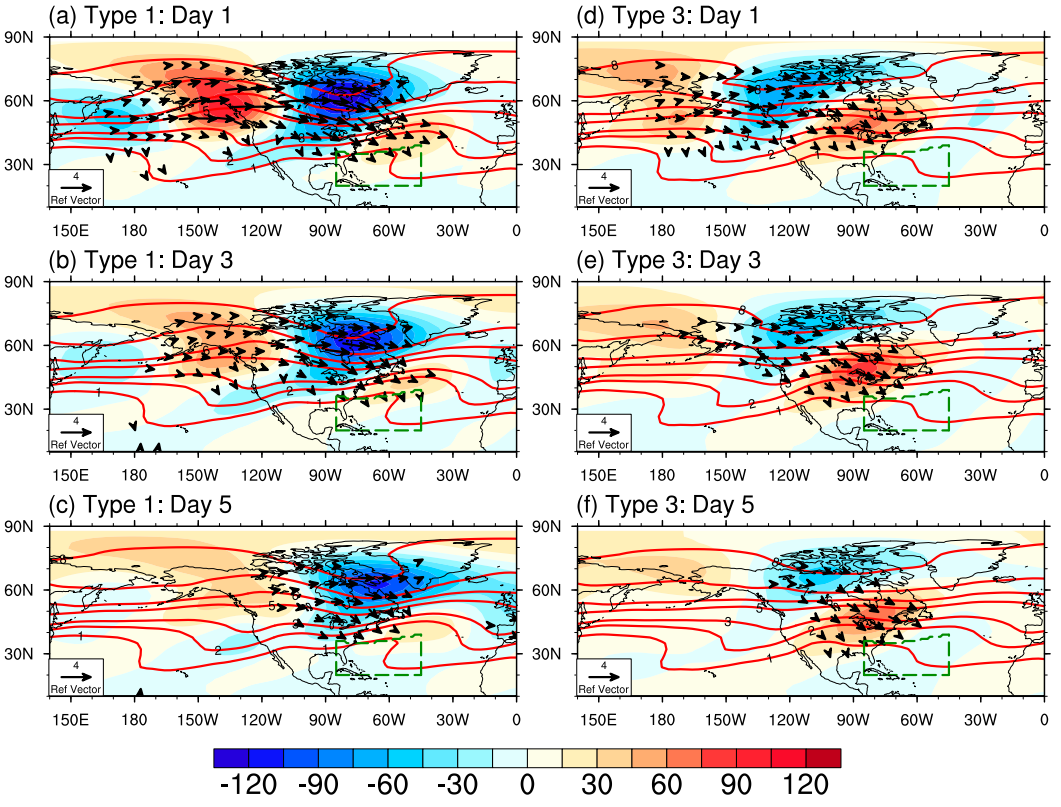

FIG. 9. Simulated evolution of type 1 and type 3 regimes: (a) 1 day, (b) 3 days, and (c) 5 days after the model initialization with the type 1 perturbations, and (d)–(f) as in (a)–(c), but for the type 3 perturbations. The color shading shows the anomalies of 200-hPa geopotential potential (m). The vectors show the wave activity flux ($m^2 s^{-2}$) (Takaya and Nakamura 2001). The small-magnitude ($<0.5\ m^2 s^{-2}$) vectors are masked out for clarity. The red contours show the PV contours between 1 and 8 PVU with an interval of 1 PVU. The green dashed lines denote the location of the high-PV tongues associated with the RWBw events.

of extratropical atmosphere anomalies. The relation between weather regimes and tropical climate modes, as well as its implications for the RWBw events, will be further investigated in the following section.

5. Modulation of weather regimes by interannual variations of tropical forcing

Tropical climate modes such as the AMM and the ENSO may affect the extratropical weather regimes in at least two ways: 1) tropical forcing may affect the occurrence counts of extratropical weather regimes, and 2) the basic-state flow variations associated with tropical forcing may modulate how weather regimes affect the evolution of the downstream flow. As suggested by sections 4a and 4b, the influences of tropical climate modes on weather regimes may contribute to variations of RWBw. We note that Cassou et al. (2005) has identified tropical influences on the weather regimes in the North Atlantic domain. However, the associations between those regimes and the RWBw events are weak (section 4b), so this section will focus on the weather regimes in the North Pacific–North America domain.

Using indices of the AMM and the ENSO, we examine whether tropical climate modes modulate the occurrence frequency of the North Pacific/North America weather regimes on the interannual scale (Table 2). The table shows that their correlations fail to reach the 95% confidence level, suggesting that the tropical modes do not strongly affect the counts of weather regimes. Using a different ENSO index, such as the Niño-3.4 index, does not increase the correlations above the 95% confidence level either (not shown). The lack of statistically significant correlations does not necessarily rule out the possibility that other tropical modes, such as the Madden–Julian oscillation (MJO), may affect the counts of those regimes. Nonetheless, the results here indicate that the counts of those weather regimes—at least on the interannual scale—are not strongly affected by the AMM or ENSO.

We now explore the possibility that the basic-state flow variations associated with tropical modes may

TABLE 2. Correlation between the seasonal counts of North Pacific/North American weather regimes and selected climate indices (Jul–Oct of 1979–2013). The AMM and Niño-4 indices are as in Table 1. None of the correlations reach the 95% confidence level. The last row shows the standard deviation of the seasonal counts of weather regimes (unit: days per season).

	Type 1	Type 2	Type 3	Type 4	Type 5	Type 6
AMM	−0.13	−0.12	0.00	0.10	−0.01	0.15
Niño-4	0.00	−0.31	0.18	−0.02	0.09	0.05
Std dev	5.05	5.32	5.88	5.37	4.88	5.67

modulate the downstream flow evolution associated with weather regimes and the frequency of RWB occurrence. We will proceed with the observational data instead of idealized simulations, as the latter does not fully capture the observed variations of the basic state in the extratropics (section 3b). Based on our interest in the RWBw events and their strong correlation with the AMM (Table 1), we focus on the potential impact of the AMM on the evolution of type 1 and type 3 regimes. More specifically, we analyze the reanalysis dataset and show the lead–lag composites of the regimes during the two phases of the AMM (Figs. 10 and 11).

Figure 10 shows the regime-related flow perturbations during both phases of the AMM. Despite these similarities between the two AMM phases, a closer inspection suggests some potentially important differences. For example, the North Pacific ridge associated with the type 1 regime is stronger during the positive phase of the AMM, and the configuration of geopotential height anomalies appear more zonal near the east coast of North America during the same phase (Figs. 10a,b,e). In comparison, the differences of type 3 perturbations appear weaker (Figs. 10c,d,f). During the negative phase of the AMM, the east coast ridge associated with the type 3 regime weakens and slightly shifts to the south. As for the basic-state zonal wind, the Rossby wave response (section 3b) to the AMM-related precipitation anomalies near the Greater Antilles (Smirnov and Vimont 2011) likely contributes to the differences near the midlatitude jet. For example, the North Atlantic jet intensifies during the negative phase of the AMM, indicating an elongated baroclinic zone over North America and potential differences of wave propagation speed. The basic-state flow differences resemble those in Fig. 4a and are consistent with the anticorrelation of the RWBw index and the AMM (Table 1). However, the flow differences only reach the 90% confidence level, suggesting large unforced variability of extratropical atmosphere.

Even though the differences of perturbations and basic-state flows are moderate, the flow evolution shows intriguing differences after three days (Fig. 11). Both type 1 and type 3 regimes show wave trains that are associated with strong wave activity flux. During the negative phase of the AMM, the wave trains appear to extend farther equatorward near 30°N, 60°W (Figs. 11e,f). Additionally, there is an anomalous convergence of wave activity flux near the east coast of North America (Figs. 11e,f), which indicates the absorption of equatorward-propagating waves associated with the subtropical RWB (Magnusdottir and Haynes 1996). Even though the wave activity flux is noisy, the differences near the coast of North America are statistically significant and appear consistent with an increase of RWBw events during the negative phase of the AMM. For example, a 5-day lag analysis similar to Fig. 8 suggests that RWBw events follow about 33% of the type 3 regime during the positive phases of the AMM, but the ratio increases to 48% during the negative phase of the AMM.

The changes of wave activity flux might be related to the flow differences near the midlatitude jet of the North Atlantic (Fig. 10). During the negative phase of the AMM, the zonal flow accelerates near 45°N but decelerates on 30°N (Figs. 10e,f). Besides increasing the anticyclonic shear near the midlatitude jet, the flow changes also affect the critical layer and the wave propagation. The critical layer indicates the region of RWB and is defined as the area where the speed of the basic-state flow ($\overline{U}$) roughly equals to the phase speed of Rossby waves (c) (Randel and Held 1991). In addition, the value of $\overline{U} - c$ is also inversely proportional to a refractive index of Rossby waves and thus modulates the wave propagation (Thorncroft et al. 1993; Hartmann and Zuercher 1998). For the breaking waves with a phase speed c of $\leq 10\,\mathrm{m\,s^{-1}}$, which is typical for RWBw events (Zhang and Wang 2018), the flow deceleration near 30°N helps to extend the critical layer and increase the refractive index over the northwestern Atlantic. The changes favor the equatorward propagation of Rossby waves and their ensuing breaking in the critical layer. Besides the upper-level flow changes near the midlatitude jet, changes of the low-level baroclinicity (Orlanski 2003; Rivière 2009) and the tropical circulation (Esler et al. 2000; Walker and Magnusdottir 2002) may also contribute to the observed variations of RWBw events. A more quantitative understanding of the wave–flow interaction will need further research.

6. Summary and discussion

Anticyclonic RWB events strongly influence Atlantic TC activity on the intraseasonal-to-seasonal scale (Zhang et al. 2016, 2017; Papin 2017; Li et al. 2018). This

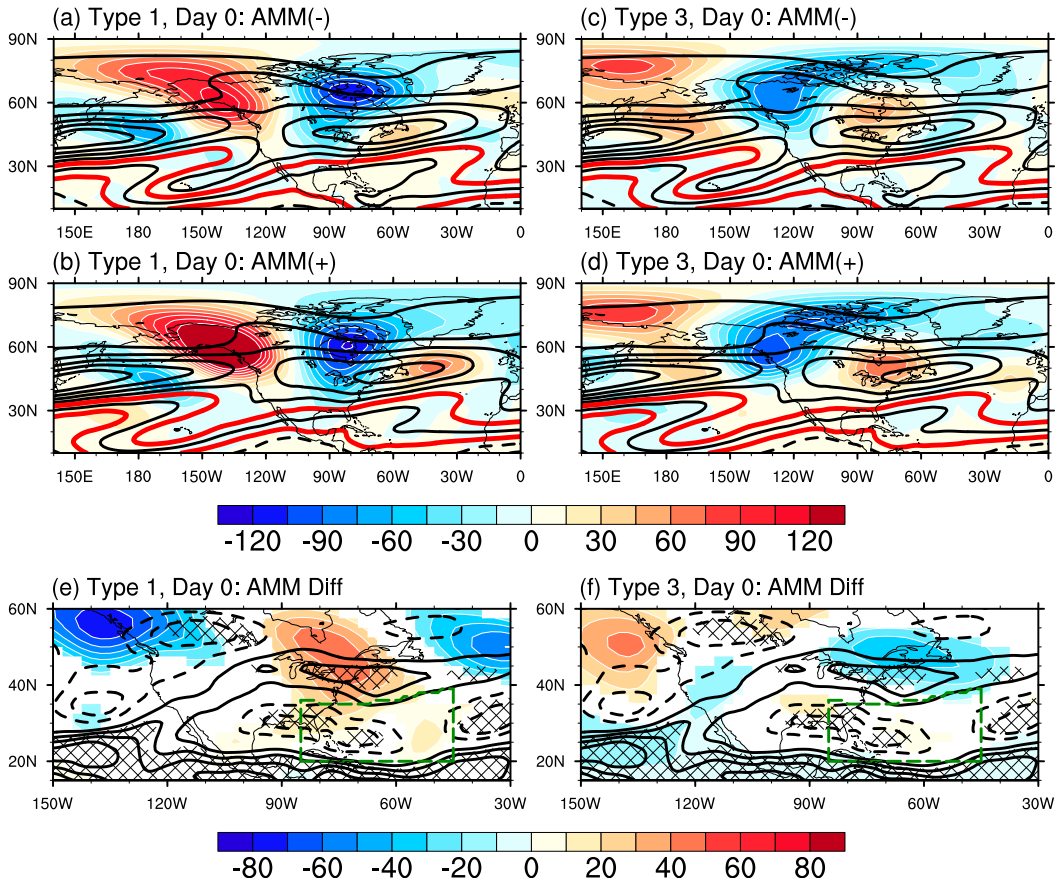

FIG. 10. Modulation of the zonal wind, type 1, and type 3 regimes by the AMM. The plots show the composites of (a),(c) the negative phase and (b),(d) the positive phase of the AMM, and (e),(f) their differences (negative minus positive). Each AMM phase includes 8 years with extreme values of the AMM index (Chiang and Vimont 2004). The color shading shows the 200-hPa geopotential height (m) anomalies associated with the (a),(b) type 1 regime and (c),(d) type 3 regime; in the same plots, the contour lines show the composites of seasonal mean 200-hPa zonal wind ($m\,s^{-1}$). In (e) and (f), the color shading shows the 90%-confidence-level differences of geopotential height anomalies; the contour lines show the differences of zonal wind with the hatching highlighting the parts *above* the 90% confidence level. The zero line of wind contours is omitted unless otherwise specified; the interval of wind contours is $5\,m\,s^{-1}$ in (a)–(d) and $1\,m\,s^{-1}$ in (e) and (f). The red contours in (a)–(d) denote the 0 and $10\,m\,s^{-1}$ wind contours on the equatorward flank of the midlatitude jet, with the region in between corresponding to the critical layer for RWBw events. The green dashed lines in (e) and (f) denote the location of the high-PV tongues associated with the RWBw events. Note that (e) and (f) show a smaller domain to highlight the differences near the western Atlantic.

study focuses on the events over the western subtropical basin (RWBw), which have relatively strong impacts on Atlantic TC activity (Zhang et al. 2017), and explores what may drive the variations. The findings suggest that the variations of the RWBw events are tied to both tropical and extratropical variations on the weather–climate continuum.

Our analyses show that variations of the RWBw events have strong associations with the SST variability of the North Atlantic. On the interannual scale, seasonal occurrences of RWBw events are strongly correlated to the AMM and the associated tropical SST anomalies, which modulate the Caribbean precipitation. Together with the central Pacific precipitation, the Caribbean precipitation influences the basic state of the atmospheric circulation over North America and the North Atlantic. The changes of the basic-state flow further modulate behaviors of extratropical Rossby waves that develop locally or propagate from remote regions. Such wave–flow interactions are complex, but their impacts on RWB events are consistent with the correlations between the tropical climate modes and seasonal occurrences of the RWBw events. On the synoptic scale, the RWBw events modulate the turbulent heat flux and

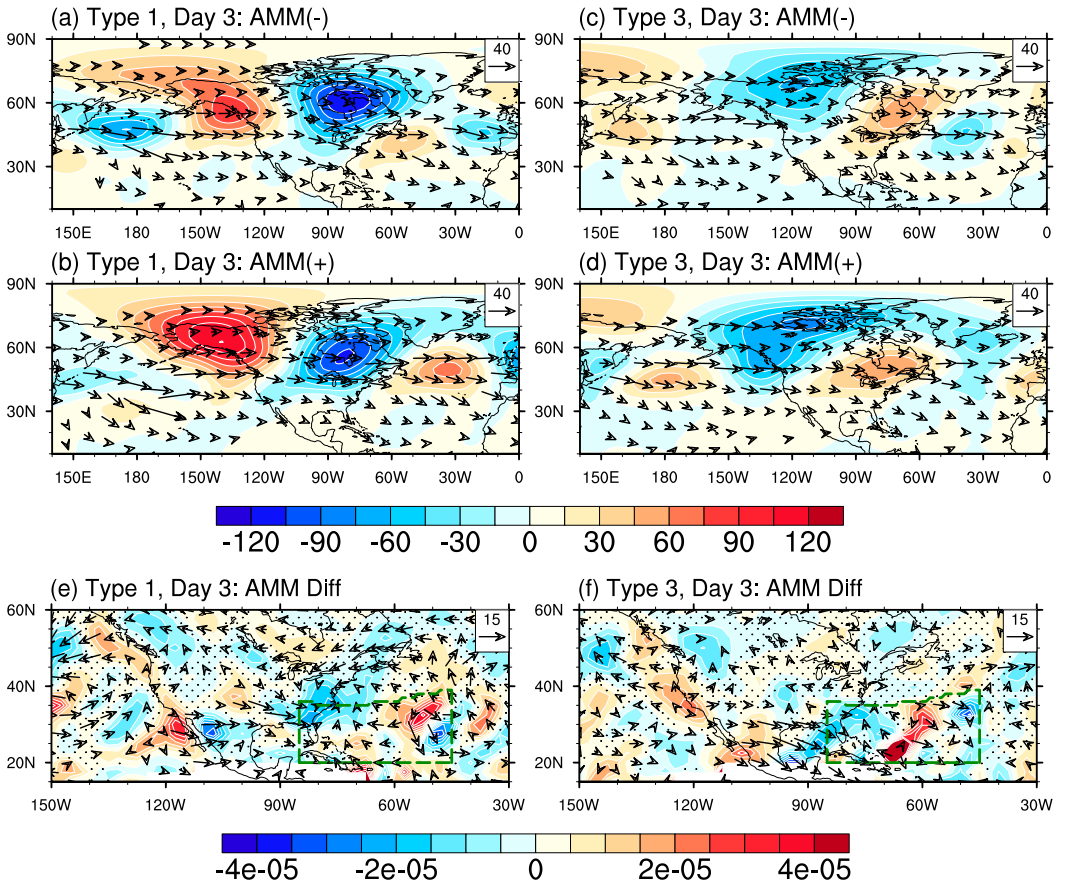

FIG. 11. Modulation of the evolution of type 1 and type 3 regimes by the AMM. The figure arrangement is similar to Fig. 10. The color shading shows the 200-hPa geopotential height (m) anomalies that lag the (a),(b) type 1 regime and (c),(d) type 3 regime by 3 days; in the same plots, the vectors show the composites of the 200-hPa wave activity fluxes ($m^2 s^{-2}$) (Takaya and Nakamura 2001). (e),(f) The vectors show the 90% confidence level differences of wave activity fluxes; the color shading shows the differences of the divergence of the wave activity flux, with stippling masking out the parts below the 90% confidence level.

the radiative heat flux at the air–sea interface. The anomalous flux contributes to SST anomalies of a horseshoe pattern, which can project on the AMM and the summertime horseshoe mode of the North Atlantic SST. Therefore, RWBw occurrence is modulated by tropical Atlantic SST, and the RWBw events actively influence the evolution of tropical SST during the hurricane season.

Nonetheless, the RWB–SST interaction could be complicated by other factors, especially the extratropical atmosphere variability, which is not simply dictated by tropical climate modes. This motivates us to investigate the extratropical atmosphere variability in the weather regime framework and their connections with RWBw. The findings suggest that the weather regimes in the North Atlantic domain are closely associated with the RWB events in the eastern basin, but their connections with the RWBw events are relatively weak. Instead, the RWBw events are closely associated with flow variations in the upstream domain of the North Pacific–North America. For example, one of the weather regimes in the domain features a wave train pattern that extends from the North Pacific to the North Atlantic, and another is associated with circulation anomalies that may involve an interaction between the Arctic region and the midlatitudes. The flow perturbations associated with the weather regimes propagate on the basic-state flow, which is subject to the influence tropical climate modes (e.g., the AMM), and contribute to the RWBw events over the North Atlantic.

The results shed light on some important issues for predicting Atlantic TC activity, such as the controversial NAO–TC relation and the prediction failure of the 2013 hurricane season. On the one hand, the weather regimes associated with the NAO are closely associated with RWB events over the eastern Atlantic but not those

over the western basin. Although all those RWB events could affect TC development, the eastern basin events show much weaker impacts on TC activity (Zhang et al. 2017). Therefore, the finding in this study helps explain why a large body of the NAO-focused studies led to inconsistent findings of the extratropical impact on Atlantic TC activity. On the other hand, the upstream flow perturbations, such as type 1 and type 3 regimes in the North Pacific–North America domain, show much stronger impacts on the RWBw events.

The findings of this study suggest two potential paths to predict the RWBw events beyond the synoptic time scale. One path is to predict the basic-state flow over North America and the North Atlantic, which could be affected by tropical forcing (e.g., SST and the MJO) and extratropical processes (e.g., sea ice). The other path is to predict upstream perturbations, especially those in the sector of the North Pacific and North America. The upstream flow is subject to the impact of extratropical processes on various time scales, as well as recurving Pacific TCs (e.g., Archambault et al. 2015), the MJO (e.g., Yoo et al. 2012), and Asian monsoons (e.g., Moon et al. 2013). The combination of different basic-state flow and initial perturbations, as discussed in section 4, could further complicate the prediction of RWB events. An accurate representation of the basic-state flow, upstream perturbations, and their interactions is likely necessary for skillful predictions of RWB events and their impact on Atlantic TC activity. The predictability of the extratropical circulation, especially during the warm season, is an area of active research (e.g., Lee et al. 2011; Ossó et al. 2018). The realization of predictability may benefit from the continuing improvements of models (e.g., Bauer et al. 2015; Yang et al. 2015), and an upcoming study will report some encouraging results.

The study has a few limitations that warrant additional remarks. Our discussion mainly focuses on the qualitative aspects due to the limitations of the idealized model and the coarse-resolution data. For example, an idealized dry model is used in the study partly because models with complex physics, such as some CMIP5 models, have trouble with simulating realistic extratropical climate during the warm season (Chang 2013). However, the idealized dry model excludes the diabatic processes that affect the life cycle of breaking waves (Zhang and Wang 2018) and the midlatitude jet stream (Shaw et al. 2016). As noted in earlier sections, the idealized model settings are likely responsible for some differences between the observations and our simulations. The differences prevent us from further exploring the relation between RWB events of the basic state of atmospheric environment. Another limitation of the study is related to the strong variations of SST and surface heat fluxes in the extratropics. Even though the atmospheric responses to the extratropical SST forcing have been considered much weaker than the unforced variability of the atmosphere (Kushnir et al. 2002; Sutton and Hodson 2007; Guemas et al. 2010), the impacts of extratropical SST forcing appear evident in new wintertime high-resolution simulations (Piazza et al. 2016; Parfitt et al. 2017) and on the decadal scale (Dong et al. 2013). A more quantitative understanding of those issues, which is beyond the scope of this study, may carry significant values for the prediction practice.

Overall, the findings of this study help illustrate that the variations of RWB events during the Atlantic hurricane season are subject to influences of both the tropical and the extratropical processes. Especially, the study outlined a potential interaction between the RWB events and the Atlantic SST, which might help reconcile the tropical and the extratropical impacts on Atlantic TC activity. Although the study focuses on the synoptic to interannual scale, our findings on the tropical–extratropical interaction might also help understand Atlantic TC activity on longer time scales. In addition, the connection between RWB events and extratropical atmosphere variability offers a new perspective to explore the predictability and uncertainties of Atlantic TC activity.

Acknowledgments. The study is supported by NOAA Grants NA15NWS4680007 and NA16OAR4310080, and NRL Grant N00173-15-1-G004. We are grateful to Drs. Gudrun Magnusdottir, Ryan Sriver, Timothy Dunkerton, Robert Jeffery Trapp, Hiroyuki Murakami, and three anonymous reviewers for helpful discussions and advice. We acknowledge the NCAR/CISL for providing computing resources and the ECMWF for making the ERA-Interim reanalysis publicly available (http://apps.ecmwf.int/datasets/).

REFERENCES

Abatzoglou, J. T., and G. Magnusdottir, 2006: Planetary wave breaking and nonlinear reflection: Seasonal cycle and interannual variability. *J. Climate*, **19**, 6139–6152, https://doi.org/10.1175/JCLI3968.1.

Adler, R. F., and Coauthors, 2003: The version-2 Global Precipitation Climatology Project (GPCP) monthly precipitation analysis (1979–present). *J. Hydrometeor.*, **4**, 1147–1167, https://doi.org/10.1175/1525-7541(2003)004<1147:TVGPCP>2.0.CO;2.

Alexander, M. A., D. J. Vimont, P. Chang, and J. D. Scott, 2010: The impact of extratropical atmospheric variability on ENSO: Testing the seasonal footprinting mechanism using coupled model experiments. *J. Climate*, **23**, 2885–2901, https://doi.org/10.1175/2010JCLI3205.1.

Appenzeller, C., and H. C. Davies, 1992: Structure of stratospheric intrusions into the troposphere. *Nature*, **358**, 570–572, https://doi.org/10.1038/358570a0.

Archambault, H. M., D. Keyser, L. F. Bosart, C. A. Davis, and J. M. Cordeira, 2015: A composite perspective of the extratropical flow response to recurving western North Pacific tropical cyclones. *Mon. Wea. Rev.*, **143**, 1122–1141, https://doi.org/10.1175/MWR-D-14-00270.1.

Ballenzweig, E. M., 1959: Relation of long-period circulation anomalies to tropical storm formation and motion. *J. Meteor.*, **16**, 121–139, https://doi.org/10.1175/1520-0469(1959)016<0121:ROLPCA>2.0.CO;2.

Barnston, A. G., and R. E. Livezey, 1987: Classification, seasonality and persistence of low-frequency atmospheric circulation patterns. *Mon. Wea. Rev.*, **115**, 1083–1126, https://doi.org/10.1175/1520-0493(1987)115<1083:CSAPOL>2.0.CO;2.

Barrier, N., C. Cassou, J. Deshayes, and A.-M. Treguier, 2014: Response of North Atlantic Ocean circulation to atmospheric weather regimes. *J. Phys. Oceanogr.*, **44**, 179–201, https://doi.org/10.1175/JPO-D-12-0217.1.

Bauer, P., A. Thorpe, and G. Brunet, 2015: The quiet revolution of numerical weather prediction. *Nature*, **525**, 47–55, https://doi.org/10.1038/nature14956.

Benedict, J. J., S. Lee, and S. B. Feldstein, 2004: Synoptic view of the North Atlantic Oscillation. *J. Atmos. Sci.*, **61**, 121–144, https://doi.org/10.1175/1520-0469(2004)061<0121:SVOTNA>2.0.CO;2.

Bentley, A. M., L. F. Bosart, and D. Keyser, 2017: Upper-tropospheric precursors to the formation of subtropical cyclones that undergo tropical transition in the North Atlantic basin. *Mon. Wea. Rev.*, **145**, 503–520, https://doi.org/10.1175/MWR-D-16-0263.1.

Bjerknes, J., 1969: Atmospheric teleconnections from the equatorial Pacific. *Mon. Wea. Rev.*, **97**, 163–172, https://doi.org/10.1175/1520-0493(1969)097<0163:ATFTEP>2.3.CO;2.

Bosart, L. F., B. J. Moore, J. M. Cordeira, and H. M. Archambault, 2017: Interactions of North Pacific tropical, midlatitude, and polar disturbances resulting in linked extreme weather events over North America in October 2007. *Mon. Wea. Rev.*, **145**, 1245–1273, https://doi.org/10.1175/MWR-D-16-0230.1.

Brunke, M. A., Z. Wang, X. Zeng, M. Bosilovich, and C.-L. Shie, 2011: An assessment of the uncertainties in ocean surface turbulent fluxes in 11 reanalysis, satellite-derived, and combined global datasets. *J. Climate*, **24**, 5469–5493, https://doi.org/10.1175/2011JCLI4223.1.

Cassou, C., C. Deser, L. Terray, J. W. Hurrell, and M. Drévillon, 2004: Summer sea surface temperature conditions in the North Atlantic and their impact upon the atmospheric circulation in early winter. *J. Climate*, **17**, 3349–3363, https://doi.org/10.1175/1520-0442(2004)017<3349:SSSTCI>2.0.CO;2.

——, L. Terray, and A. S. Phillips, 2005: Tropical Atlantic influence on European heat waves. *J. Climate*, **18**, 2805–2811, https://doi.org/10.1175/JCLI3506.1.

Chang, C.-C., and Z. Wang, 2018: Relative impacts of local and remote forcing on tropical cyclone frequency in numerical model simulations. *Geophys. Res. Lett.*, **45**, 7843–7850, https://doi.org/10.1029/2018GL078606.

Chang, E. K., 2013: CMIP5 projection of significant reduction in extratropical cyclone activity over North America. *J. Climate*, **26**, 9903–9922, https://doi.org/10.1175/JCLI-D-13-00209.1.

Chen, J.-H., and S.-J. Lin, 2013: Seasonal predictions of tropical cyclones using a 25-km-resolution general circulation model. *J. Climate*, **26**, 380–398, https://doi.org/10.1175/JCLI-D-12-00061.1.

Chiang, J. C. H., and D. J. Vimont, 2004: Analogous Pacific and Atlantic meridional modes of tropical atmosphere–ocean variability. *J. Climate*, **17**, 4143–4158, https://doi.org/10.1175/JCLI4953.1.

——, and C. M. Bitz, 2005: Influence of high latitude ice cover on the marine Intertropical Convergence Zone. *Climate Dyn.*, **25**, 477–496, https://doi.org/10.1007/s00382-005-0040-5.

Colbert, A. J., and B. J. Soden, 2012: Climatological variations in North Atlantic tropical cyclone tracks. *J. Climate*, **25**, 657–673, https://doi.org/10.1175/JCLI-D-11-00034.1.

Coumou, D., J. Lehmann, and J. Beckmann, 2015: The weakening summer circulation in the Northern Hemisphere mid-latitudes. *Science*, **348**, 324–327, https://doi.org/10.1126/science.1261768.

Czaja, A., and C. Frankignoul, 2002: Observed impact of Atlantic SST anomalies on the North Atlantic Oscillation. *J. Climate*, **15**, 606–623, https://doi.org/10.1175/1520-0442(2002)015<0606:OIOASA>2.0.CO;2.

Davis, C. A., and L. F. Bosart, 2004: The TT problem: Forecasting the tropical transition of cyclones. *Bull. Amer. Meteor. Soc.*, **85**, 1657–1662, https://doi.org/10.1175/BAMS-85-11-1657.

Dee, D. P., and Coauthors, 2011: The ERA-Interim reanalysis: Configuration and performance of the data assimilation system. *Quart. J. Roy. Meteor. Soc.*, **137**, 553–597, https://doi.org/10.1002/qj.828.

Dong, B., R. T. Sutton, T. Woollings, and K. Hodges, 2013: Variability of the North Atlantic summer storm track: Mechanisms and impacts on European climate. *Environ. Res. Lett.*, **8**, 034037, https://doi.org/10.1088/1748-9326/8/3/034037.

Drouard, M., G. Rivière, and P. Arbogast, 2013: The North Atlantic Oscillation response to large-scale atmospheric anomalies in the northeastern Pacific. *J. Atmos. Sci.*, **70**, 2854–2874, https://doi.org/10.1175/JAS-D-12-0351.1.

——, ——, and ——, 2015: The link between the North Pacific climate variability and the North Atlantic Oscillation via downstream propagation of synoptic waves. *J. Climate*, **28**, 3957–3976, https://doi.org/10.1175/JCLI-D-14-00552.1.

Dunstone, N. J., D. M. Smith, and R. Eade, 2011: Multi-year predictability of the tropical Atlantic atmosphere driven by the high latitude North Atlantic Ocean. *Geophys. Res. Lett.*, **38**, L14701, https://doi.org/10.1029/2011GL047949.

Elsner, J. B., 2003: Tracking hurricanes. *Bull. Amer. Meteor. Soc.*, **84**, 353–356, https://doi.org/10.1175/BAMS-84-3-353.

Esler, J. G., L. M. Polvani, and R. A. Plumb, 2000: The effect of a Hadley circulation on the propagation and reflection of planetary waves in a simple one-layer model. *J. Atmos. Sci.*, **57**, 1536–1556, https://doi.org/10.1175/1520-0469(2000)057<1536:TEOAHC>2.0.CO;2.

Ferranti, L., T. N. Palmer, F. Molteni, and E. Klinker, 1990: Tropical-extratropical interaction associated with the 30–60 day oscillation and its impact on medium and extended range prediction. *J. Atmos. Sci.*, **47**, 2177–2199, https://doi.org/10.1175/1520-0469(1990)047<2177:TEIAWT>2.0.CO;2.

Fischer, M. S., B. H. Tang, and K. L. Corbosiero, 2017: Assessing the influence of upper-tropospheric troughs on tropical cyclone intensification rates after genesis. *Mon. Wea. Rev.*, **145**, 1295–1313, https://doi.org/10.1175/MWR-D-16-0275.1.

Folland, C. K., J. Knight, H. W. Linderholm, D. Fereday, S. Ineson, and J. W. Hurrell, 2009: The summer North Atlantic Oscillation: Past, present, and future. *J. Climate*, **22**, 1082–1103, https://doi.org/10.1175/2008JCLI2459.1.

Franzke, C., S. Lee, and S. B. Feldstein, 2004: Is the North Atlantic Oscillation a breaking wave? *J. Atmos. Sci.*, **61**, 145–160, https://doi.org/10.1175/1520-0469(2004)061<0145:ITNAOA>2.0.CO;2.

Funatsu, B. M., and D. W. Waugh, 2008: Connections between potential vorticity intrusions and convection in the eastern tropical Pacific. *J. Atmos. Sci.*, **65**, 987–1002, https://doi.org/10.1175/2007JAS2248.1.

Galarneau, T. J., R. McTaggart-Cowan, L. F. Bosart, and C. A. Davis, 2015: Development of North Atlantic tropical disturbances near upper-level potential vorticity streamers. *J. Atmos. Sci.*, **72**, 572–597, https://doi.org/10.1175/JAS-D-14-0106.1.

Gill, A. E., 1980: Some simple solutions for heat-induced tropical circulation. *Quart. J. Roy. Meteor. Soc.*, **106**, 447–462, https://doi.org/10.1002/qj.49710644905.

Goldenberg, S. B., and L. J. Shapiro, 1996: Physical mechanisms for the association of El Niño and West African rainfall with Atlantic major hurricane activity. *J. Climate*, **9**, 1169–1187, https://doi.org/10.1175/1520-0442(1996)009<1169:PMFTAO>2.0.CO;2.

——, C. W. Landsea, A. M. Mestas-Nuñez, and W. M. Gray, 2001: The recent increase in Atlantic hurricane activity: Causes and implications. *Science*, **293**, 474–479, https://doi.org/10.1126/science.1060040.

Gordon, C. T., and W. F. Stern, 1982: A description of the GFDL global spectral model. *Mon. Wea. Rev.*, **110**, 625–644, https://doi.org/10.1175/1520-0493(1982)110<0625:ADOTGG>2.0.CO;2.

Gray, W. M., 1984a: Atlantic seasonal hurricane frequency. Part I: El Niño and 30 mb quasi-biennial oscillation influences. *Mon. Wea. Rev.*, **112**, 1649–1668, https://doi.org/10.1175/1520-0493(1984)112<1649:ASHFPI>2.0.CO;2.

——, 1984b: Atlantic seasonal hurricane frequency. Part II: Forecasting its variability. *Mon. Wea. Rev.*, **112**, 1669–1683, https://doi.org/10.1175/1520-0493(1984)112<1669:ASHFPI>2.0.CO;2.

Guemas, V., D. Salas-Mélia, M. Kageyama, H. Giordani, A. Voldoire, and E. Sanchez-Gomez, 2010: Summer interactions between weather regimes and surface ocean in the North-Atlantic region. *Climate Dyn.*, **34**, 527–546, https://doi.org/10.1007/s00382-008-0491-6.

Häkkinen, S., P. B. Rhines, and D. L. Worthen, 2011: Atmospheric blocking and Atlantic multidecadal ocean variability. *Science*, **334**, 655–659, https://doi.org/10.1126/science.1205683.

Hall, N. M. J., 2000: A simple GCM based on dry dynamics and constant forcing. *J. Atmos. Sci.*, **57**, 1557–1572, https://doi.org/10.1175/1520-0469(2000)057<1557:ASGBOD>2.0.CO;2.

Hanley, D., J. Molinari, and D. Keyser, 2001: A composite study of the interactions between tropical cyclones and upper-tropospheric troughs. *Mon. Wea. Rev.*, **129**, 2570–2584, https://doi.org/10.1175/1520-0493(2001)129<2570:ACSOTI>2.0.CO;2.

Hartmann, D. L., and P. Zuercher, 1998: Response of baroclinic life cycles to barotropic shear. *J. Atmos. Sci.*, **55**, 297–313, https://doi.org/10.1175/1520-0469(1998)055<0297:ROBLCT>2.0.CO;2.

Held, I. M., M. Ting, and H. Wang, 2002: Northern winter stationary waves: Theory and modeling. *J. Climate*, **15**, 2125–2144, https://doi.org/10.1175/1520-0442(2002)015<2125:NWSWTA>2.0.CO;2.

Jones, P. D., T. Jónsson, and D. Wheeler, 1997: Extension to the North Atlantic Oscillation using early instrumental pressure observations from Gibraltar and south-west Iceland. *Int. J. Climatol.*, **17**, 1433–1450, https://doi.org/10.1002/(SICI)1097-0088(19971115)17:13<1433::AID-JOC203>3.0.CO;2-P.

Kao, H., and J. Yu, 2009: Contrasting eastern-Pacific and central-Pacific types of ENSO. *J. Climate*, **22**, 615–632, https://doi.org/10.1175/2008JCLI2309.1.

Kiladis, G. N., 1998: Observations of Rossby waves linked to convection over the eastern tropical Pacific. *J. Atmos. Sci.*, **55**, 321–339, https://doi.org/10.1175/1520-0469(1998)055<0321:OORWLT>2.0.CO;2.

——, and K. M. Weickmann, 1992: Circulation anomalies associated with tropical convection during northern winter. *Mon. Wea. Rev.*, **120**, 1900–1923, https://doi.org/10.1175/1520-0493(1992)120<1900:CAAWTC>2.0.CO;2.

Kossin, J. P., S. J. Camargo, and M. Sitkowski, 2010: Climate modulation of North Atlantic hurricane tracks. *J. Climate*, **23**, 3057–3076, https://doi.org/10.1175/2010JCLI3497.1.

Kushnir, Y., W. A. Robinson, I. Bladé, N. M. J. Hall, S. Peng, and R. Sutton, 2002: Atmospheric GCM response to extratropical SST anomalies: Synthesis and evaluation. *J. Climate*, **15**, 2233–2256, https://doi.org/10.1175/1520-0442(2002)015<2233:AGRTES>2.0.CO;2.

Landsea, C. W., and J. L. Franklin, 2013: Atlantic hurricane database uncertainty and presentation of a new database format. *Mon. Wea. Rev.*, **141**, 3576–3592, https://doi.org/10.1175/MWR-D-12-00254.1.

Lau, K., and L. Peng, 1992: Dynamics of atmospheric teleconnections during the northern summer. *J. Climate*, **5**, 140–158, https://doi.org/10.1175/1520-0442(1992)005<0140:DOATDT>2.0.CO;2.

Lee, J.-Y., B. Wang, Q. Ding, K.-J. Ha, J.-B. Ahn, A. Kumar, B. Stern, and O. Alves, 2011: How predictable is the Northern Hemisphere summer upper-tropospheric circulation? *Climate Dyn.*, **37**, 1189–1203, https://doi.org/10.1007/s00382-010-0909-9.

Leroux, M., M. Plu, and F. Roux, 2016: On the sensitivity of tropical cyclone intensification under upper-level trough forcing. *Mon. Wea. Rev.*, **144**, 1179–1202, https://doi.org/10.1175/MWR-D-15-0224.1.

Li, W., Z. Wang, G. Zhang, M. S. Peng, S. G. Benjamin, and M. Zhao, 2018: Subseasonal variability of Rossby wave breaking and impacts on tropical cyclones during the North Atlantic warm season. *J. Climate*, **31**, 9679–9695, https://doi.org/10.1175/JCLI-D-17-0880.1.

Li, X., S.-P. Xie, S. T. Gille, and C. Yoo, 2016: Atlantic-induced pan-tropical climate change over the past three decades. *Nat. Climate Change*, **6**, 275–279, https://doi.org/10.1038/nclimate2840.

Lian, T., and D. Chen, 2012: An evaluation of rotated EOF analysis and its application to tropical Pacific SST variability. *J. Climate*, **25**, 5361–5373, https://doi.org/10.1175/JCLI-D-11-00663.1.

Ling, J., and C. Zhang, 2013: Diabatic heating profiles in recent global reanalyses. *J. Climate*, **26**, 3307–3325, https://doi.org/10.1175/JCLI-D-12-00384.1.

Magnusdottir, G., and P. H. Haynes, 1996: Wave activity diagnostics applied to baroclinic wave life cycles. *J. Atmos. Sci.*, **53**, 2317–2353, https://doi.org/10.1175/1520-0469(1996)053<2317:WADATB>2.0.CO;2.

McIntyre, M. E., and T. N. Palmer, 1983: Breaking planetary waves in the stratosphere. *Nature*, **305**, 593–600, https://doi.org/10.1038/305593a0.

Michel, C., and G. Rivière, 2011: The link between Rossby wave breakings and weather regime transitions. *J. Atmos. Sci.*, **68**, 1730–1748, https://doi.org/10.1175/2011JAS3635.1.

Molinari, J., and D. Vollaro, 1989: External influences on hurricane intensity. Part I: Outflow layer eddy angular momentum fluxes. *J. Atmos. Sci.*, **46**, 1093–1105, https://doi.org/10.1175/1520-0469(1989)046<1093:EIOHIP>2.0.CO;2.

Moon, J.-Y., B. Wang, K.-J. Ha, and J.-Y. Lee, 2013: Teleconnections associated with Northern Hemisphere summer monsoon intraseasonal oscillation. *Climate Dyn.*, **40**, 2761–2774, https://doi.org/10.1007/s00382-012-1394-0.

Murakami, H., G. Villarini, G. A. Vecchi, W. Zhang, and R. Gudgel, 2016: Statistical–dynamical seasonal prediction of North Atlantic and U.S. landfalling tropical cyclones using the high-resolution GFDL FLOR coupled model. *Mon. Wea. Rev.*, **144**, 2101–2123, https://doi.org/10.1175/MWR-D-15-0308.1.

Orlanski, I., 2003: Bifurcation in eddy life cycles: Implications for storm track variability. *J. Atmos. Sci.*, **60**, 993–1023, https://doi.org/10.1175/1520-0469(2003)60<993:BIELCI>2.0.CO;2.

——, 2005: A new look at the Pacific storm track variability: Sensitivity to tropical SSTs and to upstream seeding. *J. Atmos. Sci.*, **62**, 1367–1390, https://doi.org/10.1175/JAS3428.1.

Ossó, A., R. Sutton, L. Shaffrey, and B. Dong, 2018: Observational evidence of European summer weather patterns predictable from spring. *Proc. Natl. Acad. Sci. USA*, **115**, 59–63, https://doi.org/10.1073/pnas.1713146114.

Papin, P. P., 2017: Variations in potential vorticity streamer activity: Development pathways, environmental impacts, and links to tropical cyclone activity in the North Atlantic basin. Ph.D. dissertation, The State University of New York at Albany, 226 pp., https://search.proquest.com/openview/bcc1d48dc74c82096977fb1d27956a22.

Parfitt, R., A. Czaja, and Y.-O. Kwon, 2017: The impact of SST resolution change in the ERA-Interim reanalysis on wintertime Gulf Stream frontal air–sea interaction. *Geophys. Res. Lett.*, **44**, 3246–3254, https://doi.org/10.1002/2017GL073028.

Patricola, C. M., R. Saravanan, and P. Chang, 2014: The impact of the El Niño–Southern Oscillation and Atlantic meridional mode on seasonal Atlantic tropical cyclone activity. *J. Climate*, **27**, 5311–5328, https://doi.org/10.1175/JCLI-D-13-00687.1.

Peirano, C., K. Corbosiero, and B. Tang, 2016: Revisiting trough interactions and tropical cyclone intensity change. *Geophys. Res. Lett.*, **43**, 5509–5515, https://doi.org/10.1002/2016GL069040.

Peters, D., and D. W. Waugh, 1996: Influence of barotropic shear on the poleward advection of upper-tropospheric air. *J. Atmos. Sci.*, **53**, 3013–3031, https://doi.org/10.1175/1520-0469(1996)053<3013:IOBSOT>2.0.CO;2.

Piazza, M., L. Terray, J. Boé, E. Maisonnave, and E. Sanchez-Gomez, 2016: Influence of small-scale North Atlantic sea surface temperature patterns on the marine boundary layer and free troposphere: A study using the atmospheric ARPEGE model. *Climate Dyn.*, **46**, 1699–1717, https://doi.org/10.1007/s00382-015-2669-z.

Postel, G. A., and M. H. Hitchman, 1999: A climatology of Rossby wave breaking along the subtropical tropopause. *J. Atmos. Sci.*, **56**, 359–373, https://doi.org/10.1175/1520-0469(1999)056<0359:ACORWB>2.0.CO;2.

Randel, W. J., and I. M. Held, 1991: Phase speed spectra of transient eddy fluxes and critical layer absorption. *J. Atmos. Sci.*, **48**, 688–697, https://doi.org/10.1175/1520-0469(1991)048<0688:PSSOTE>2.0.CO;2.

Ray, P., and C. Zhang, 2010: A case study of the mechanics of extratropical influence on the initiation of the Madden–Julian oscillation. *J. Atmos. Sci.*, **67**, 515–528, https://doi.org/10.1175/2009JAS3059.1.

Rayner, N. A., D. E. Parker, E. B. Horton, C. K. Folland, L. V. Alexander, D. P. Rowell, E. C. Kent, and A. Kaplan, 2003: Global analyses of sea surface temperature, sea ice, and night marine air temperature since the late nineteenth century. *J. Geophys. Res.*, **108**, 4407, https://doi.org/10.1029/2002JD002670.

Rivière, G., 2009: Effect of latitudinal variations in low-level baroclinicity on eddy life cycles and upper-tropospheric wave-breaking processes. *J. Atmos. Sci.*, **66**, 1569–1592, https://doi.org/10.1175/2008JAS2919.1.

——, 2011: A dynamical interpretation of the poleward shift of the jet streams in global warming scenarios. *J. Atmos. Sci.*, **68**, 1253–1272, https://doi.org/10.1175/2011JAS3641.1.

——, and I. Orlanski, 2007: Characteristics of the Atlantic storm-track eddy activity and its relation with the North Atlantic Oscillation. *J. Atmos. Sci.*, **64**, 241–266, https://doi.org/10.1175/JAS3850.1.

Rodwell, M. J., and B. J. Hoskins, 2001: Subtropical anticyclones and summer monsoons. *J. Climate*, **14**, 3192–3211, https://doi.org/10.1175/1520-0442(2001)014<3192:SAASM>2.0.CO;2.

Ryoo, J., Y. Kaspi, D. W. Waugh, G. N. Kiladis, D. E. Waliser, E. J. Fetzer, and J. Kim, 2013: Impact of Rossby wave breaking on U.S. West Coast winter precipitation during ENSO events. *J. Climate*, **26**, 6360–6382, https://doi.org/10.1175/JCLI-D-12-00297.1.

Sabbatelli, T. A., and M. E. Mann, 2007: The influence of climate state variables on Atlantic tropical cyclone occurrence rates. *J. Geophys. Res.*, **112**, D17114, https://doi.org/10.1029/2007JD008385.

Sardeshmukh, P. D., and B. J. Hoskins, 1988: The generation of global rotational flow by steady idealized tropical divergence. *J. Atmos. Sci.*, **45**, 1228–1251, https://doi.org/10.1175/1520-0469(1988)045<1228:TGOGRF>2.0.CO;2.

Schubert, S., H. Wang, and M. Suarez, 2011: Warm season subseasonal variability and climate extremes in the Northern Hemisphere: The role of stationary Rossby waves. *J. Climate*, **24**, 4773–4792, https://doi.org/10.1175/JCLI-D-10-05035.1.

Shaw, T. A., and Coauthors, 2016: Storm track processes and the opposing influences of climate change. *Nat. Geosci.*, **9**, 656–664, https://doi.org/10.1038/ngeo2783.

Smirnov, D., and D. J. Vimont, 2011: Variability of the Atlantic meridional mode during the Atlantic hurricane season. *J. Climate*, **24**, 1409–1424, https://doi.org/10.1175/2010JCLI3549.1.

——, and ——, 2012: Extratropical forcing of tropical Atlantic variability during boreal summer and fall. *J. Climate*, **25**, 2056–2076, https://doi.org/10.1175/JCLI-D-11-00104.1.

Smith, D. M., R. Eade, N. J. Dunstone, D. Fereday, J. M. Murphy, H. Pohlmann, and A. A. Scaife, 2010: Skillful multi-year predictions of Atlantic hurricane frequency. *Nat. Geosci.*, **3**, 846–849, https://doi.org/10.1038/ngeo1004.

Strong, C., and G. Magnusdottir, 2008: Tropospheric Rossby wave breaking and the NAO/NAM. *J. Atmos. Sci.*, **65**, 2861–2876, https://doi.org/10.1175/2008JAS2632.1.

——, and ——, 2009: The role of tropospheric Rossby wave breaking in the Pacific decadal oscillation. *J. Climate*, **22**, 1819–1833, https://doi.org/10.1175/2008JCLI2593.1.

Sutton, R. T., and D. L. R. Hodson, 2005: Atlantic Ocean forcing of North American and European summer climate. *Science*, **309**, 115–118, https://doi.org/10.1126/science.1109496.

——, and ——, 2007: Climate response to basin-scale warming and cooling of the North Atlantic Ocean. *J. Climate*, **20**, 891–907, https://doi.org/10.1175/JCLI4038.1.

Swenson, E. T., and D. M. Straus, 2017: Rossby wave breaking and transient eddy forcing during Euro-Atlantic circulation regimes. *J. Atmos. Sci.*, **74**, 1735–1755, https://doi.org/10.1175/JAS-D-16-0263.1.

Takaya, K., and H. Nakamura, 2001: A formulation of a phase-independent wave-activity flux for stationary and migratory

quasigeostrophic eddies on a zonally varying basic flow. *J. Atmos. Sci.*, **58**, 608–627, https://doi.org/10.1175/1520-0469(2001)058<0608:AFOAPI>2.0.CO;2.

Thorncroft, C. D., B. J. Hoskins, and M. E. McIntyre, 1993: Two paradigms of baroclinic-wave life-cycle behaviour. *Quart. J. Roy. Meteor. Soc.*, **119**, 17–55, https://doi.org/10.1002/qj.49711950903.

Tomaziello, A. C. N., L. M. V. Carvalho, and A. W. Gandu, 2016: Intraseasonal variability of the Atlantic Intertropical Convergence Zone during austral summer and winter. *Climate Dyn.*, **47**, 1717–1733, https://doi.org/10.1007/s00382-015-2929-y.

Trenberth, K. E., G. W. Branstator, D. Karoly, A. Kumar, N.-C. Lau, and C. Ropelewski, 1998: Progress during TOGA in understanding and modeling global teleconnections associated with tropical sea surface temperatures. *J. Geophys. Res.*, **103**, 14 291–14 324, https://doi.org/10.1029/97JC01444.

Tyrlis, E., and B. J. Hoskins, 2008: The morphology of Northern Hemisphere blocking. *J. Atmos. Sci.*, **65**, 1653–1665, https://doi.org/10.1175/2007JAS2338.1.

Vavrus, S. J., F. Wang, J. E. Martin, J. A. Francis, Y. Peings, and J. Cattiaux, 2017: Changes in North American atmospheric circulation and extreme weather: Influence of Arctic amplification and Northern Hemisphere snow cover. *J. Climate*, **30**, 4317–4333, https://doi.org/10.1175/JCLI-D-16-0762.1.

Vecchi, G. A., and Coauthors, 2014: On the seasonal forecasting of regional tropical cyclone activity. *J. Climate*, **27**, 7994–8016, https://doi.org/10.1175/JCLI-D-14-00158.1.

Vigaud, N., and A. W. Robertson, 2017: Convection regimes and tropical-midlatitude interactions over the Intra-American Seas from May to November. *Int. J. Climatol.*, **37**, 987–1000, https://doi.org/10.1002/joc.5051.

Vimont, D. J., and J. P. Kossin, 2007: The Atlantic meridional mode and hurricane activity. *Geophys. Res. Lett.*, **34**, L07709, https://doi.org/10.1029/2007GL029683.

Vitart, F., and Coauthors, 2007: Dynamically-based seasonal predictions of Atlantic tropical storm activity issued in June by EUROSIP. *Geophys. Res. Lett.*, **34**, L16815, https://doi.org/10.1029/2007GL030740.

Walker, C. C., and G. Magnusdottir, 2002: Effect of the Hadley circulation on the reflection of planetary waves in three-dimensional tropospheric flows. *J. Atmos. Sci.*, **59**, 2846–2859, https://doi.org/10.1175/1520-0469(2002)059<2846:EOTHCO>2.0.CO;2.

——, and T. Schneider, 2006: Eddy influences on Hadley circulations: Simulations with an idealized GCM. *J. Atmos. Sci.*, **63**, 3333–3350, https://doi.org/10.1175/JAS3821.1.

Wang, J., J. Zhang, E. Watanabe, M. Ikeda, K. Mizobata, J. E. Walsh, X. Bai, and B. Wu, 2009: Is the Dipole Anomaly a major driver to record lows in Arctic summer sea ice extent? *Geophys. Res. Lett.*, **36**, L05706, https://doi.org/10.1029/2008GL036706.

Woollings, T., B. Hoskins, M. Blackburn, and P. Berrisford, 2008: A new Rossby wave–breaking interpretation of the North Atlantic Oscillation. *J. Atmos. Sci.*, **65**, 609–626, https://doi.org/10.1175/2007JAS2347.1.

Yang, X., and Coauthors, 2015: Seasonal predictability of extratropical storm tracks in GFDL's high-resolution climate prediction model. *J. Climate*, **28**, 3592–3611, https://doi.org/10.1175/JCLI-D-14-00517.1.

Yoo, C., S. Lee, and S. B. Feldstein, 2012: Arctic response to an MJO-like tropical heating in an idealized GCM. *J. Atmos. Sci.*, **69**, 2379–2393, https://doi.org/10.1175/JAS-D-11-0261.1.

Zhang, G., and Z. Wang, 2013: Interannual variability of the Atlantic Hadley circulation in boreal summer and its impacts on tropical cyclone activity. *J. Climate*, **26**, 8529–8544, https://doi.org/10.1175/JCLI-D-12-00802.1.

——, and ——, 2018: North Atlantic extratropical Rossby wave breaking during the warm season: Wave life cycle and role of diabatic heating. *Mon. Wea. Rev.*, **146**, 695–712, https://doi.org/10.1175/MWR-D-17-0204.1.

——, ——, T. J. Dunkerton, M. S. Peng, and G. Magnusdottir, 2016: Extratropical impacts on Atlantic tropical cyclone activity. *J. Atmos. Sci.*, **73**, 1401–1418, https://doi.org/10.1175/JAS-D-15-0154.1.

——, ——, M. S. Peng, and G. Magnusdottir, 2017: Characteristics and impacts of extratropical Rossby wave breaking during the Atlantic hurricane season. *J. Climate*, **30**, 2363–2379, https://doi.org/10.1175/JCLI-D-16-0425.1.